Supporting information for

Topological control in paddlewheel metal-organic cages via ligand length variation

Steven Tsoukatos,[a] Ashakiran Maibam,[b] Ravichandar Babarao[b,c] and Witold M. Bloch[a]

[a]College of Science & Engineering, Flinders University, Sturt Road, Bedford Park, SA 5042, Australia. Email: witold.bloch@flinders.edu.au

[b]School of Science, Centre for Advanced Materials and Industrial Chemistry (CAMIC), RMIT University, Melbourne, 3001 Victoria, Australia.

[c]CSIRO, Clayton 3168, Victoria, Australia.

Table of contents

1. Experimental section

1.1. Materials and measurements

Unless otherwise stated, all chemicals were obtained from commercial sources and used as received. NMR experiments were performed either on a Bruker Avance Neo NMR spectrometer operating at 400 MHz or on a Bruker Avance III NMR spectrometer operating at 600 MHz. The deuterated solvent used was either d_6-DMSO, $CDCl_3$, or d_7-DMF. Chemical shifts were recorded in ppm. Spectra were calibrated by assignment of the residual solvent peak to δ_H 2.50 for d_6-DMSO, δ_H 7.26 for $CDCl_3$, and δ_H 8.03 for d_7-DMF. Coupling constants (J) were recorded in Hz. Infrared spectra were collected on a Perkin-Elmer Spectrum 100 using an ATR sampling accessory. Thermal gravimetric analysis (TGA) was performed on Perkin-Elmer TGA 800. Powder X-ray diffraction (PXRD) data were collected on a Bruker Advance D8 diffractometer (capillary stage) using Cu Kα radiation (λ = 1.5418 Å) or on a Bruker D8 Advance Eco diffractometer (capillary stage) using Co Kα radiation (λ = 1.7902 Å). 0.8 mm or 1.0 mm capillaries were filled with the respective solvent before loading crystals of the samples. This was done to avoid any possible desolvation of the crystalline sample. Simulated PXRD patterns were generated from the single crystal data using Mercury 2023.4.330. Gas sorption isotherm measurements were performed on a Micromeritics 3Flex Surface Characterisation Analyser. UHP grade (99.999 %) N_2 and HP grade (99.995%) CO_2 was used for all measurements. Temperatures were maintained at 77 K or 195 K using a cryo-cooler on the Micromeritics 3Flex Surface Characterisation Analyser. The isotherms were then analysed to determine the Brunauer Emmett-Teller (BET) surface area using the MicroActive software (Version 3.00, Micromeritics Instrument Corp. 2013). Ligands 9,10-dimethoxyphenanthrene,[1] 1,1'-(9,10-dimethoxyphenanthrene-3,6-diyl)bis(ethan-1-one),[1] 3,6-dibromo-9,10-dimethoxyphenanthrene,[2] 3,6-dibromo-9,10-dipropoxyphenanthrene,[3] were prepared according to previously published procedures.

1.2. Synthesis of ligands

Scheme 1

*1.2.1. 9,10-dimethoxyphenanthrene-3,6-dicarboxylic acid (**L¹H₂**)*

L¹H_2 was prepared according to a literature procedure with minor alteration.[4] $Ca(ClO)_2$ (3.68 g, 25.74 mmol, 8.3 equiv.) was stirred in DI H_2O (5 mL) at 60 °C for 10 mins and cooled to 25 °C. To the mixture, Na_2CO_3 (2.74 g, 25.85 mmol, 8.3 equiv.) and NaOH (0.79 g, 19.75 mmol, 6.4 equiv.) in DI H_2O (5 mL) was added dropwise and then heated at 60 °C for 5 mins. The solution was collected by vacuum filtration and stirred at 60 °C. To the solution, 1,1'-(9,10-dimethoxyphenanthrene-3,6-diyl)bis(ethan-1-one) (1.00 g, 3.10 mmol, 1 equiv.) in 1,4-dioxane (15 mL) was added dropwise and then heated at 70 °C for 3 h. The reaction mixture was cooled to 25 °C, an aqueous saturated solution of $NaHSO_3$ (25 mL) was added, and the mixture was stirred for 1 h at 25 °C. The reaction mixture was acidified to pH = 2 with 5 % HCl. The precipitate was collected by vacuum filtration and washed with DI H_2O (5 × 25 mL) and Et_2O (2 × 5 mL). After drying at 80 °C for 16 h, **L¹H₂** was afforded as a pale-yellow powder (Yield: 0.41 g, 40 %). ^{1}H NMR (600 MHz, d_6-DMSO) δ 13.30 (s, 1H), 9.27 (d, J = 1.5 Hz, 1H), 8.29 (d, J = 8.5 Hz, 1H), 8.22 (dd, J = 8.5, 1.5 Hz, 1H), 4.07 (s, 3H). ^{13}C NMR (151 MHz, d_6-DMSO) δ 167.26, 144.83, 131.63, 128.64, 127.45, 127.43, 124.30, 122.63, 61.13. ν_{max} (neat, cm^{-1}): 2946 (br), 1688 (s), 1607 (m), 1420 (m), 1292 (s), 1058 (s). ESI-MS: calculated for $C_{18}H_{13}O_6$ $[M\text{-}H]^-$ 325.0712, found 325.0763.

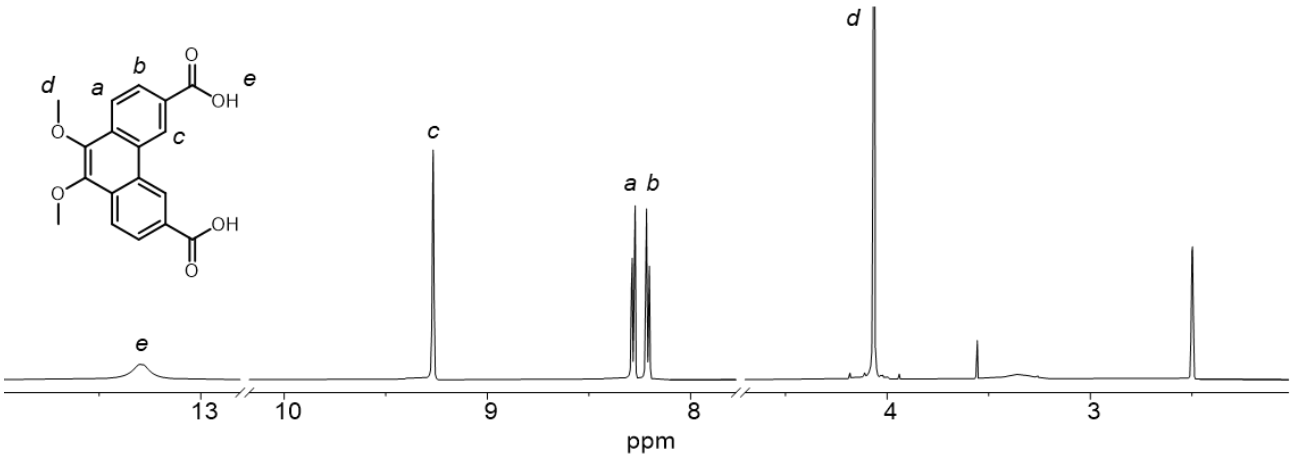

Figure S1. ^{1}H NMR spectrum (600 MHz/d_6-DMSO) of compound **L^1H_2**.

*1.2.2. 4,4'-(9,10-dimethoxyphenanthrene-3,6-diyl)dibenzoic acid (**L^2H_2**)*

3,6-dibromo-9,10-dimethoxyphenanthrene (0.26 g, 0.66 mmol, 1 equiv.), 4-carboxyphenylboronic acid (0.29 g, 1.75 mmol, 2.7 equiv.), and K_2CO_3 (1.16 g, 8.39 mmol, 12.7 equiv.) in DI H_2O (7 mL), were combined in dry DMF (32 mL). After the mixture was degassed with argon (30 mins), [$Pd(PPh_3)_4$] (100 mg, 0.087 mmol, 0.13 equiv.) was added and the mixture was stirred at 100 °C for 16 h. The reaction mixture was cooled to 25 °C and diluted with DI H_2O (50 mL). The aqueous layer was collected, washed with DCM (3 × 50 mL) and acidified to pH = 3 with 32 % HCl. The precipitate was collected by vacuum filtration and washed with DI H_2O (5 × 25 mL). After drying at 95 °C for 16 h, **L^2H_2** was afforded as a pale-yellow powder (Yield: 0.22 g, 81 %). ^{1}H NMR (600 MHz, d_6-DMSO) δ 13.01 (s, 2H), 9.29 (d, J = 1.9 Hz, 2H), 8.30 (d, J = 8.5 Hz, 2H), 8.11 (m, 8H), 8.07 (dd, J = 8.5, 1.9 Hz, 2H), 4.18 (t, J = 6.5 Hz, 4H), 1.90 (h, J = 7.1 Hz, 4H), 1.12 (t, J = 7.4 Hz, 6H). ^{13}C NMR (151 MHz, d_6-DMSO) δ 167.22, 144.26, 143.58, 136.92, 129.91, 129.65, 128.68, 128.47, 127.56, 126.33, 122.76, 121.85, 61.02. ν_{max} (neat, cm^{-1}): 2952 (br), 1693 (s), 1604 (s), 1422 (m), 1289 (s), 1074 (s). ESI-MS: calculated for $C_{30}H_{21}O_6$ $[M\text{-}H]^-$ 477.1338, found 477.1381.

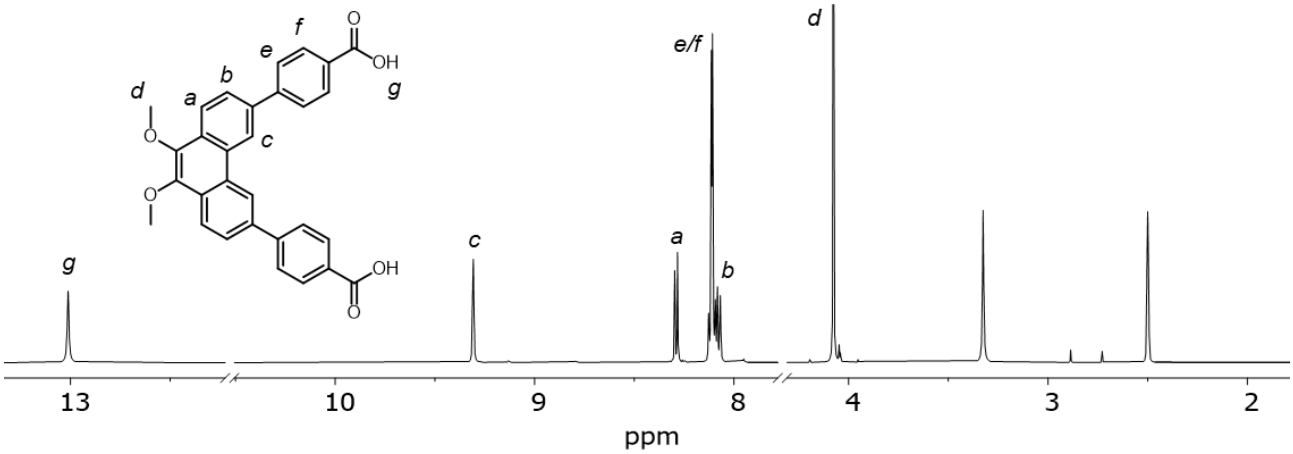

Figure S2. ^{1}H NMR spectrum (600 MHz/d_6-DMSO) of compound **L^2H_2**.

*1.2.3. 4,4'-((9,10-dimethoxyphenanthrene-3,6-diyl)bis(ethyne-2,1-diyl))dibenzoic acid (**L^3H_2**)*

To a solution of 3,6-dibromo-9,10-dimethoxyphenanthrene (0.50 g, 1.25 mmol, 1 equiv.) and methyl 4-ethynlbenzoate (0.45 g, 2.80 mmol, 2.3 equiv.) dissolved in dry THF (15 mL), diisopropyl amine (5 mL) was added. After the mixture was degassed with argon (30 mins), $Pd(PPh_3)_2Cl_2$ (80 mg, 0.114 mmol, 0.1 equiv.) and CuI (12 mg, 0.063 mmol, 0.05 equiv.) were added and the mixture was stirred at 75 °C for 16 h. The reaction mixture was cooled to 25 °C, the solvent was removed via rotary evaporation, and the resulting solid was collected and washed with Et_2O (2 × 10 mL) to afford crude

dimethyl 4,4'-((9,10-dimethoxyphenanthrene-3,6-diyl)bis(ethyne-2,1-diyl))dibenzoate as a pale yellow powder (Yield: 0.1550 g, 22 %). To a solution of crude dimethyl 4,4'-((9,10-dimethoxyphenanthrene-3,6-diyl)bis(ethyne-2,1-diyl))dibenzoate (0.15 g, 0.27 mmol, 1 equiv.) in THF (21 mL) and MeOH (6 mL), KOH (0.13 g, 2.32 mmol, 8.6 equiv.) in DI H_2O (4 mL) was added. The reaction mixture was stirred at 40 °C for 2 h, during which the precipitate slowly dissolved. The reaction mixture was cooled to 25 °C, the solvent removed via rotary evaporation, the resulting solid redispersed in DI H_2O (20 mL), and acidified to pH = 3 with 10% HCl. The precipitate was collected by vacuum filtration and washed with DI H_2O (5 × 25 mL). After drying at 80 °C for 16 h, **L^3H_2** was afforded as a pale-yellow powder (Yield: 0.14 g, 95 %). ^{1}H NMR (600 MHz, d_6-DMSO) δ 13.18 (s, 1H), 9.21 (d, J = 1.7 Hz, 1H), 8.23 (d, J = 8.5 Hz, 1H), 8.03 (d, J = 8.1 Hz, 2H), 7.88 (dd, J = 8.5, 1.4 Hz, 1H), 7.78 (d, J = 8.2 Hz, 2H), 4.07 (s, 3H). ^{13}C NMR (151 MHz, d_6-DMSO) δ 166.69, 144.19, 131.58, 130.61, 129.95, 129.64, 128.84, 127.50, 127.28, 126.70, 122.47, 119.80, 92.56, 89.50, 61.09. ν_{max} (neat, cm^{-1}): 2943 (br), 2207 (w), 1691 (s), 1603 (s), 1420 (m), 1282 (s), 1061 (s). ESI-MS: calculated for $C_{34}H_{21}O_6$ [M-H]$^-$ 525.1338, found 525.1396.

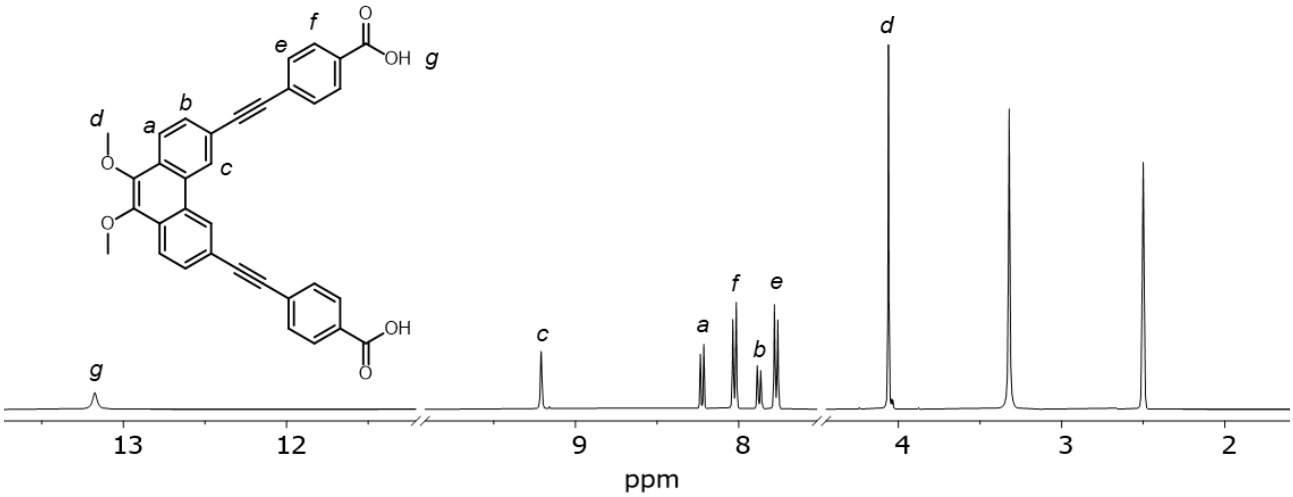

Figure S3. ^{1}H NMR spectrum (600 MHz/d_6-DMSO) of compound **L^3H_2**.

*1.2.4. 4,4'-(9,10-dipropoxyphenanthrene-3,6-diyl)dibenzoic acid (**$L^{p2}H_2$**)*

3,6-dibromo-9,10-dipropoxyphenanthrene (0.26 g, 0.57 mmol, 1 equiv.), 4-carboxyphenylboronic acid (0.29 g, 1.75 mmol, 3.1 equiv.), and K_2CO_3 (1.16 g, 8.39 mmol, 14.7 equiv.) in DI H_2O (7 mL), were combined in dry DMF (32 mL). After the mixture was degassed with argon (30 mins), [$Pd(PPh_3)_4$] (100 mg, 0.087 mmol, 0.15 equiv.) was added and the mixture was stirred at 100 °C for 16 h. The reaction mixture was cooled to 25 °C and diluted with DI H_2O (50 mL). The aqueous layer was collected, washed with DCM (3 × 50 mL) acidified to pH = 3 with 32 % HCl. The precipitate was collected by vacuum filtration and washed with DI H_2O (5 × 25 mL). After drying at 80 °C for 16 h, **$L^{p2}H_2$** was afforded as a pale-yellow powder (Yield: 0.16 g, 50 %). ^{1}H NMR (600 MHz, d_6-DMSO) δ 13.01 (s, 2H), 9.29 (d, J = 1.9 Hz, 2H), 8.30 (d, J = 8.5 Hz, 2H), 8.11 (m, 8H), 8.07 (dd, J = 8.5, 1.9 Hz, 2H), 4.18 (t, J = 6.5 Hz, 4H), 1.90 (h, J = 7.1 Hz, 4H), 1.12 (t, J = 7.4 Hz, 6H). ^{13}C NMR (151 MHz, d_6-DMSO) δ 167.43, 143.88, 142.74, 136.97, 130.68, 129.87, 128.84, 128.67, 127.43, 126.30, 122.76, 121.77, 74.80, 23.20, 10.71. ν_{max} (neat, cm^{-1}): 2968 (br), 1683 (s), 1607 (m), 1426 (s), 1288 (s), 1073 (s). ESI-MS: calculated for $C_{34}H_{30}O_6$ [M-H]$^-$ 534.2043, found 534.1984.

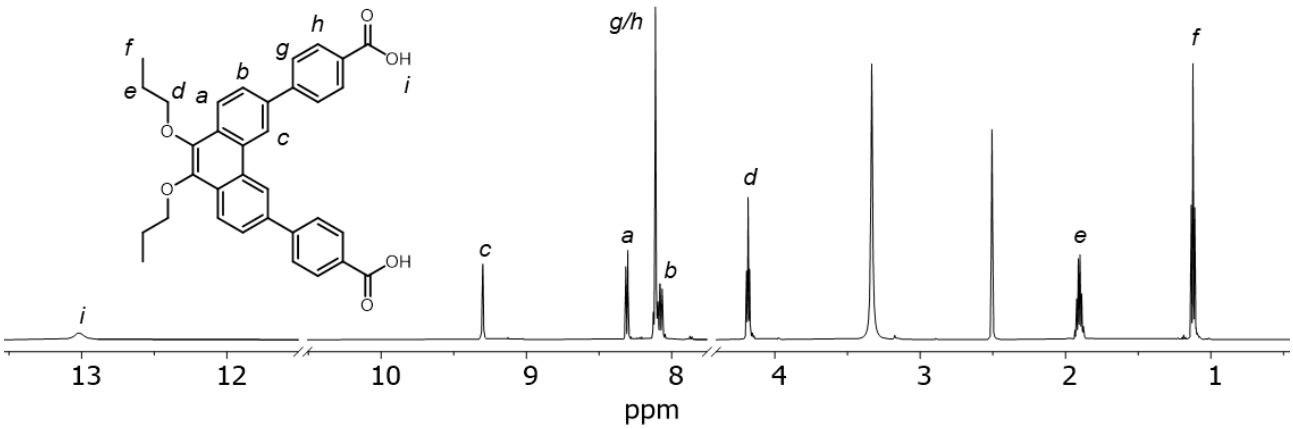

Figure S4. ^{1}H NMR spectrum (600 MHz/d_6-DMSO) of compound **$L^{p2}H_2$**.

*1.2.5. 4,4'-((9,10-dipropoxyphenanthrene-3,6-diyl)bis(ethyne-2,1-diyl))dibenzoic acid (**$L^{p3}H_2$**)*

To a solution of 3,6-dibromo-9,10-dipropoxyphenanthrene (0.56 g, 1.24 mmol, 1 equiv.) and methyl 4-ethynlbenzoate (0.45 g, 2.80 mmol, 2.3 equiv.) dissolved in dry THF (15 mL), diisopropyl amine (5 mL) was added. After the mixture was degassed with argon (30 mins), $Pd(PPh_3)_2Cl_2$ (80 mg, 0.114 mmol, 0.1 equiv.) and CuI (12 mg, 0.063 mmol, 0.05 equiv.) were added and the mixture was stirred at 75 °C for 48 h. The reaction mixture was cooled to 25 °C, the solvent was removed via rotary evaporation, and the resulting solid was collected and washed with Et_2O (2 × 10 mL) to afford crude 4,4'-((9,10-dipropoxyphenanthrene-3,6-diyl)bis(ethyne-2,1-diyl))dibenzoate as an orange-brown solid which was used without further purification (Yield: 164.9 mg, 22 %). To a solution of crude 4,4'-((9,10-dipropoxyphenanthrene-3,6-diyl)bis(ethyne-2,1-diyl))dibenzoate (0.16 g, 0.26 mmol, 1 equiv.) in THF (21 mL) and MeOH (6 mL), KOH (0.13 g, 2.32 mmol, 8.9 equiv.) in DI H_2O (4 mL) was added, and the solution was stirred at 40 °C for 2 h. The reaction solution was cooled to 25 °C, the solvent removed via rotary evaporation, the resulting solid redispersed in DI H_2O (20 mL), and acidified to pH = 3 with 10% HCl. The precipitate was collected by vacuum filtration and washed with MeOH (5 × 20 mL), aqueous 2M NaOH (1 × 10 mL), DI H_2O (1 × 5 mL), 2M HCl (1 × 20 mL) and MeOH (1 × 20 mL). After drying at 80 °C for 16 h, **$L^{p3}H_2$** was afforded as an orange powder (Yield: 75.5 mg, 48 %). ^{1}H NMR (600 MHz, d_6-DMSO) δ 13.17 (s, 1H), 9.20 (s, 1H), 8.23 (d, J = 8.4 Hz, 1H), 8.02 (d, J = 8.5 Hz, 2H), 7.87 (d, J = 8.3 Hz, 1H), 7.77 (d, J = 8.6 Hz, 2H), 4.16 (t, J = 6.5 Hz, 2H), 1.89 (h, J = 7.1 Hz, 2H), 1.10 (t, J = 7.4 Hz, 3H). ^{13}C NMR (151 MHz, d_6-DMSO) δ 166.70, 143.45, 131.57, 130.60, 129.89, 129.63, 129.23, 127.48, 127.24, 126.72, 122.49, 119.69, 92.61, 89.46, 74.91, 23.15, 10.64. ν_{max} (neat, cm^{-1}): 2959 (br), 2206 (w), 1689 (s), 1603 (s), 1417 (m), 1280 (s), 1067 (m). ESI-MS: calculated for $C_{38}H_{30}O_6$ $[M-H]^-$ 582.2043, found 582.1977.

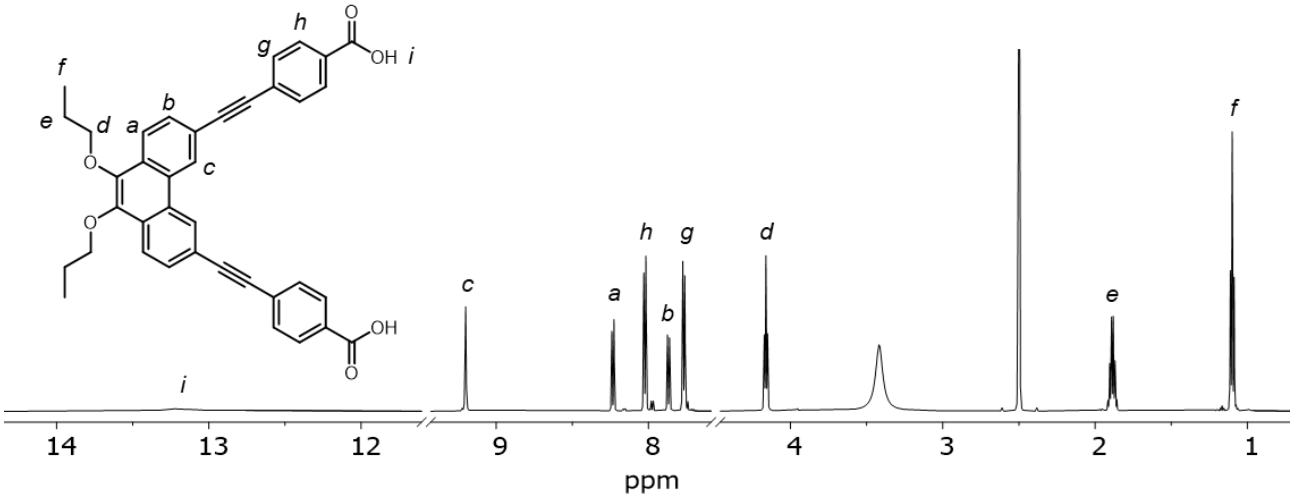

Figure S5. ^{1}H NMR spectrum (600 MHz/d_6-DMSO) of compound **$L^{p3}H_2$**.

1.3. Synthesis of MOCs

*1.3.1. Synthesis of [Cu_8(**L^1**)$_8$] (**1·Cu**)*

In a screw-cap vial, **L^1H_2** (37.3 mg, 0.11 mmol) was combined with $Cu(OAc)_2 \cdot H_2O$ (20.6 mg, 0.10 mmol) in DMF (2 mL). The solution was heated at 100 °C for 16 h, and then allowed to cool to 25 °C. After standing at 25 °C for 3 days open to air, green plate-like crystals suitable for SXCRD analysis were isolated. The crystals were washed by re-suspending in fresh MeOH (5 × 5 mL) followed by consecutive centrifugation and dried under high-vacuum to afford **1·Cu** as green plate-like crystals (Yield: 20.6 mg, 53 %). ν_{max} (neat, cm^{-1}): 1606 (s), 1393 (s), 1312 (w), 1234 (m), 1061 (s).

*1.3.2. Synthesis of [Cu_8(**L^2**)$_8$] (**2·Cu**)*

In a screw-cap vial, **L^2H_2** (25.0 mg, 0.05 mmol) was combined with $Cu(OAc)_2 \cdot H_2O$ (18.0 mg, 0.09 mmol) in DEA (3.5 mL). The solution was sonicated until full dissolution and allowed to stand at 25 °C for 3 days open to air. Blue rod-like crystals suitable for SXCRD analysis were isolated. The crystals were washed by re-suspending in fresh MeOH (5 × 5 mL) followed by consecutive centrifugation and dried under high-vacuum to afford **2·Cu** as blue rod-like crystals (Yield: 10.3 mg, 36 %). ν_{max} (neat, cm^{-1}): 1600 (s), 1397 (s), 1321 (w), 1243 (m), 1072 (s).

*1.3.3. Synthesis of [Cu_6(**L^3**)$_6$] (**3·Cu**)*

In a screw-cap vial, **L^3H_2** (35.7 mg, 0.07 mmol) was combined with $Cu(NO_3)_2 \cdot 3H_2O$ (15.5 mg, 0.06 mmol) in DMF (20 mL). The solution was allowed to stand at 25 °C for 16 h, which yielded green block crystals that were isolated and suitable for SXCRD analysis. The crystals were washed by re-suspending in fresh MeOH (5 × 5 mL) followed by consecutive centrifugation and dried under high-vacuum to afford **3·Cu** as green block crystals (Yield: 18.0 mg, 74 %). ν_{max} (neat, cm^{-1}): 2190 (w), 1602 (s), 1389 (s), 1349 (w), 1235 (m), 1061 (s).

*1.3.4. Synthesis of [Rh_8(**L^1**)$_8$] (**1·Rh**)*

In a screw-cap vial **L^1H_2** (52.8 mg, 0.16 mmol, 2 equiv.) was combined with $[Rh_2(OAc)_4]$ (35.3 mg, 0.08 mmol, 1 equiv.) and anhydrous Na_2CO_3 (16.9 mg, 0.16 mmol, 2 equiv.) in 6 mL of dry and degassed DMA. The vial was placed into a sand bath in an oven set to 100 °C and left to heat for 2 d. After allowing to cool to room temperature, the resulting emerald-green solution was separated from the solids by centrifugation, and the supernatant was combined with 20 mL of H_2O, causing a precipitate to form immediately. The precipitate was isolated by centrifugation and the supernatant was discarded. The solid was washed by re-suspending in fresh MeOH (5 × 5 mL), DMF (2 × 0.5 mL) and acetone (2 × 5 mL) followed by consecutive centrifugation and dried under high-vacuum to afford **1·Rh** as a green powder (Yield: 21.4 mg, 16 %). Single crystals of suitable quality for SCXRD were grown by heating a sealed solution of **1·Rh** in DMA at 80 °C for 5 d. ^{1}H NMR (600 MHz, d_6-DMSO) δ = 9.29 (s, 2H), 9.15 (s, 2H), 8.32 (d, J = 8.7 Hz, 2H), 8.24 (d, J = 8.6 Hz, 2H), 7.91 (d, J = 8.6 Hz, 2H), 7.79 (d, J = 8.7 Hz, 2H), 4.00 (s, 6H), 3.76 (s, 6H). ν_{max} (neat, cm^{-1}): 1613 (m), 1386 (s), 1314 (w), 1236 (m), 1061 (s).

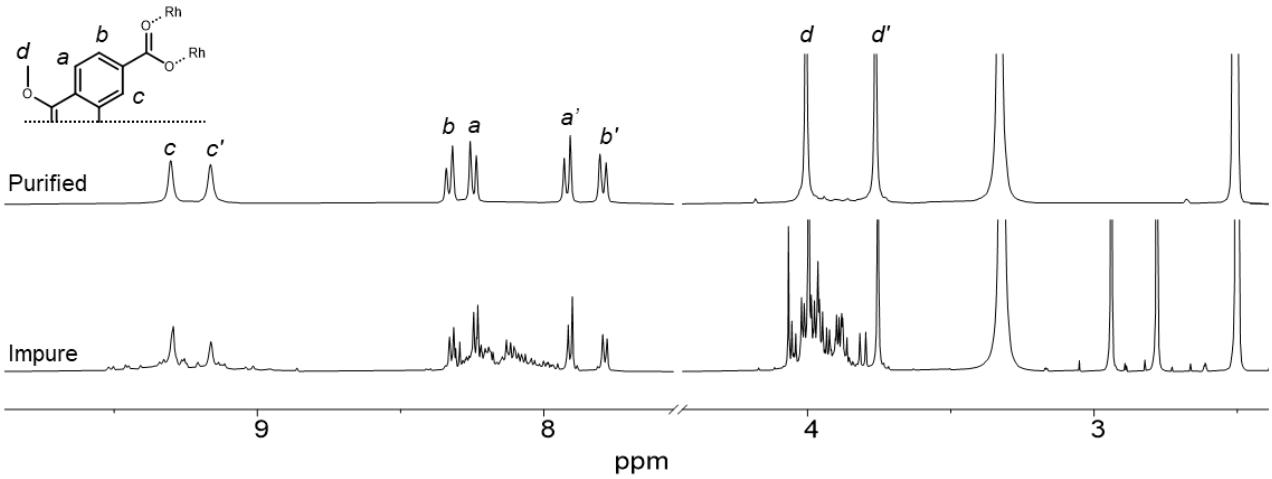

Figure S6. ^{1}H NMR spectra (600 MHz/d_6-DMSO) of **1·Rh**, both impure and purified; the symmetry of cage results in peak splitting observed. Note, that heating the reaction mixture at 100 °C for longer periods (>48 h) resulted in more complex ^{1}H NMR spectra, suggesting that other self-assembled isomers, such as the square or triangle lie on similar energetic minima.

*1.3.5. Synthesis of [Rh$_8$(**L^{p2}**)$_8$] (**2·Rh**)*

In a screw-cap vial **L^{p2}H$_2$** (86.6 mg, 0.16 mmol, 2 equiv.) was combined with [Rh$_2$(OAc)$_4$] (35.3 mg, 0.08 mmol, 1 equiv.) and anhydrous Na_2CO_3 (16.9 mg, 0.16 mmol, 2 equiv.) in 6 mL of dry and degassed DMA. The vial was placed into a sand bath in an oven set to 100 °C and left to heat for 2 d. After allowing to cool to room temperature, the resulting emerald-green solution was separated from the solids by centrifugation, and the supernatant was combined with 20 mL of MeOH, causing a precipitate to form immediately. The precipitate was isolated by centrifugation and the supernatant was discarded. The solid was washed by re-suspending in fresh MeOH, followed by consecutive centrifugation (5 × 5 mL) and dried under high-vacuum to afford **2·Rh** as a green powder (Yield: 60.2 mg, 61 %). Single crystals of suitable quality for SCXRD were grown by slow-vapour diffusion of acetone into a solution of **2·Rh** in DMA. ^{1}H NMR (600 MHz, d_7-DMF): δ 9.33 (s, 2H), 8.33 (s, 2H), 8.06 (m, 10H), 4.21 (s, 4H), 1.94 (s, 4H), 1.15 (s, 6H). ν_{max} (neat, cm^{-1}): 1592 (s), 1389 (s), 1320 (m), 1243 (w), 1069 (m).

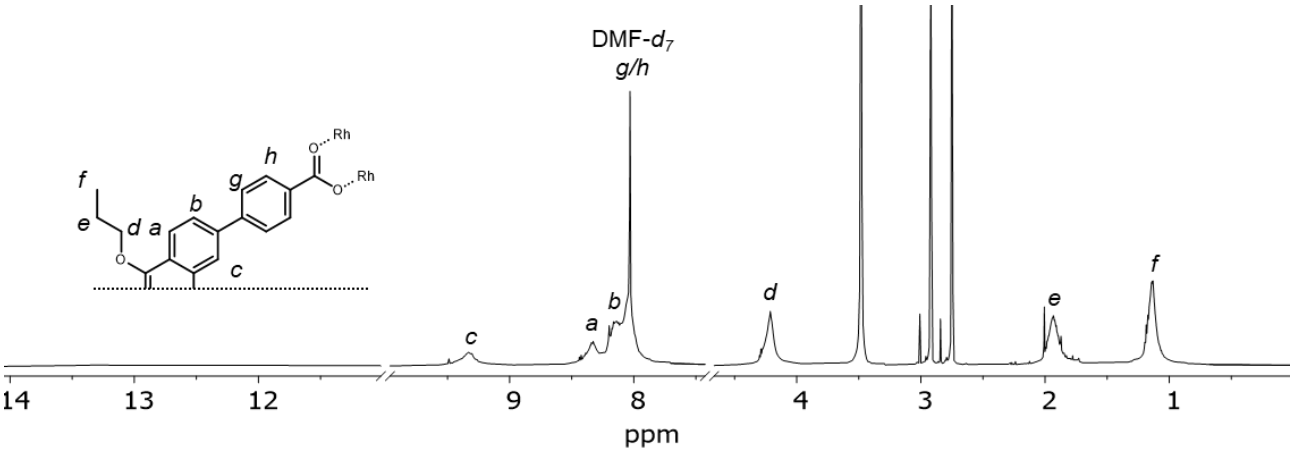

Figure S7. ^{1}H NMR spectrum (600 MHz/d_7-DMF) of compound **2·Rh**, proton peaks g and h overlap with the d_7-DMF reference peak.

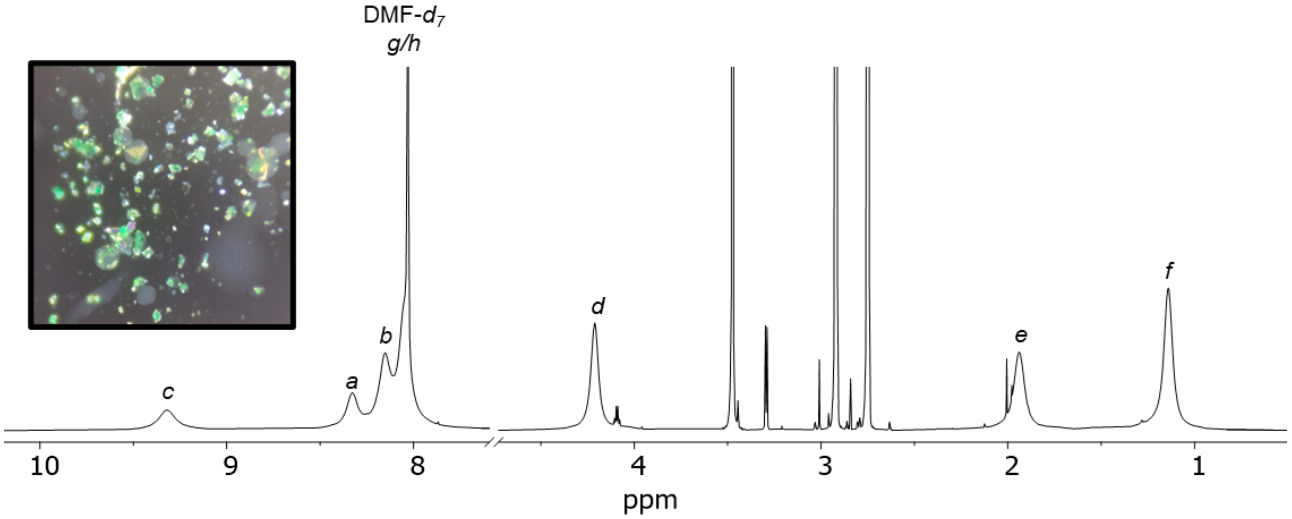

Figure S8. ^{1}H NMR spectrum (600 MHz/d_7-DMF) of compound **2·Rh** collected from crystals grown by slow-vapour diffusion of acetone into a solution of **2·Rh** in DMA, after washing the crystals with MeOH (5 × 1 mL) followed by subsequent drying under high-vacuum, demonstrating an identical spectrum to the as synthesised sample.

*1.3.6. Synthesis of [Rh_8(**$L^{p3}H_2$**)$_8$] (**3·Rh**)*

The attempted synthesis of **3·Rh** was carried out following the same conditions employed for **1·Rh** and **2·Rh**, using **$L^{p3}H_2$** at the appropriate molar quantity. ^{1}H NMR analysis of the resulting precipitate revealed the isolation of a complex mixture, which despite our best efforts, was unable to be purified.

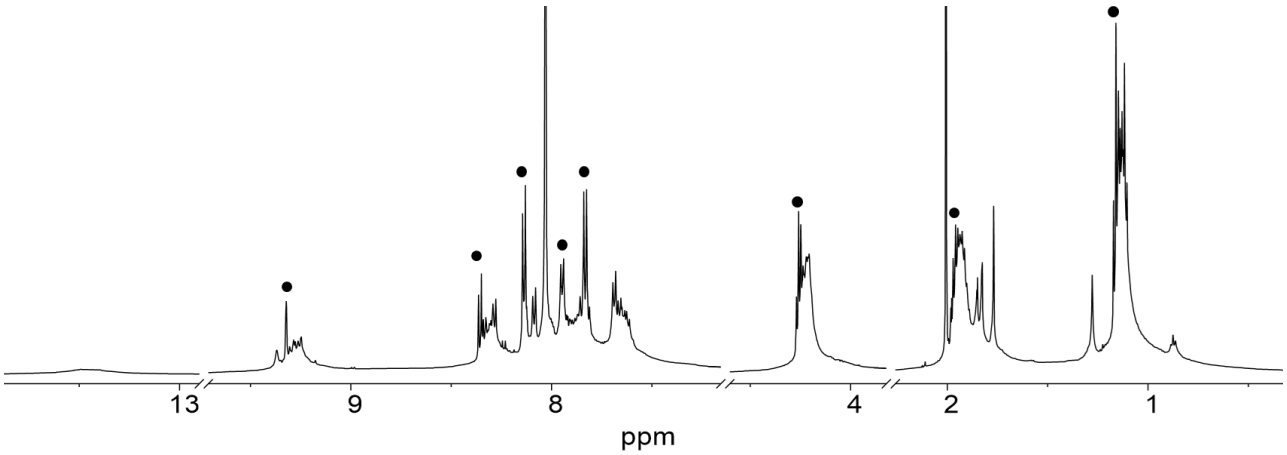

Figure S9. ^{1}H NMR spectrum (600 MHz/d_7-DMF) of isolated precipitate from attempted **3·Rh** synthesis. Peaks associated with the free ligand are indicated (●).

2. Powder X-ray diffraction

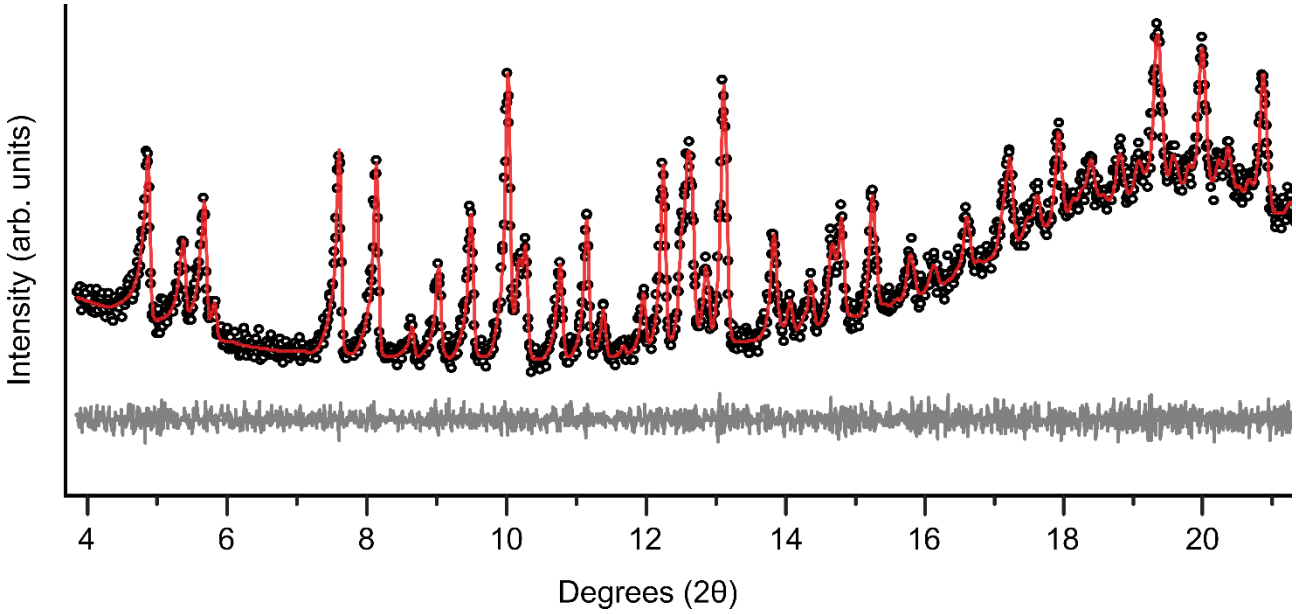

Figure S10. Rietveld refinement of the PXRD pattern of **1·Cu**. Refinement cell parameters: Monoclinic $P2_1/m$, a = 19.67 Å; b = 30.31 Å; c = 19.73 Å; α = 90°; β = 113.10°; γ = 90°. For comparison, the cell parameters of the X-ray structure are: a = 19.34 Å; b = 29.81 Å; c = 19.58 Å; α = 90°; β = 113.53°; γ = 90°.

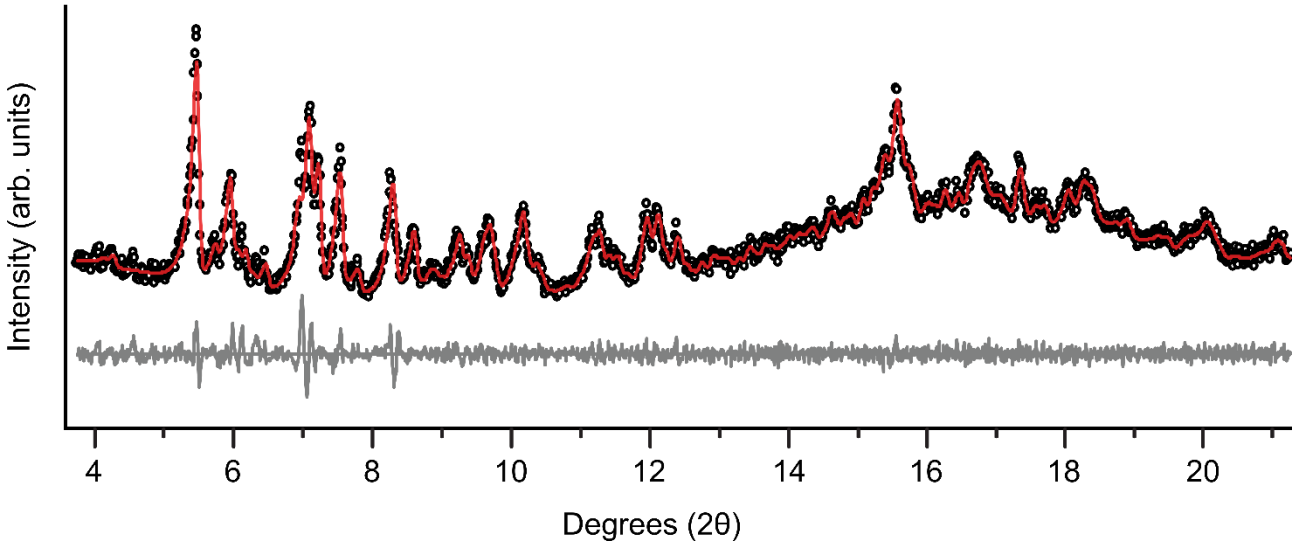

Figure S11. Rietveld refinement of the PXRD pattern of **2·Cu**. Refined parameters: Monoclinic $P2_1/c$, a = 29.36 Å; b = 54.22 Å; c = 31.83 Å; α = 90°; β = 98.39°; γ = 90°. For comparison, the cell parameters of the X-ray structure are: a = 28.77 Å; b = 53.90 Å; c = 31.40 Å; α = 90°; β = 97.11°; γ = 90°.

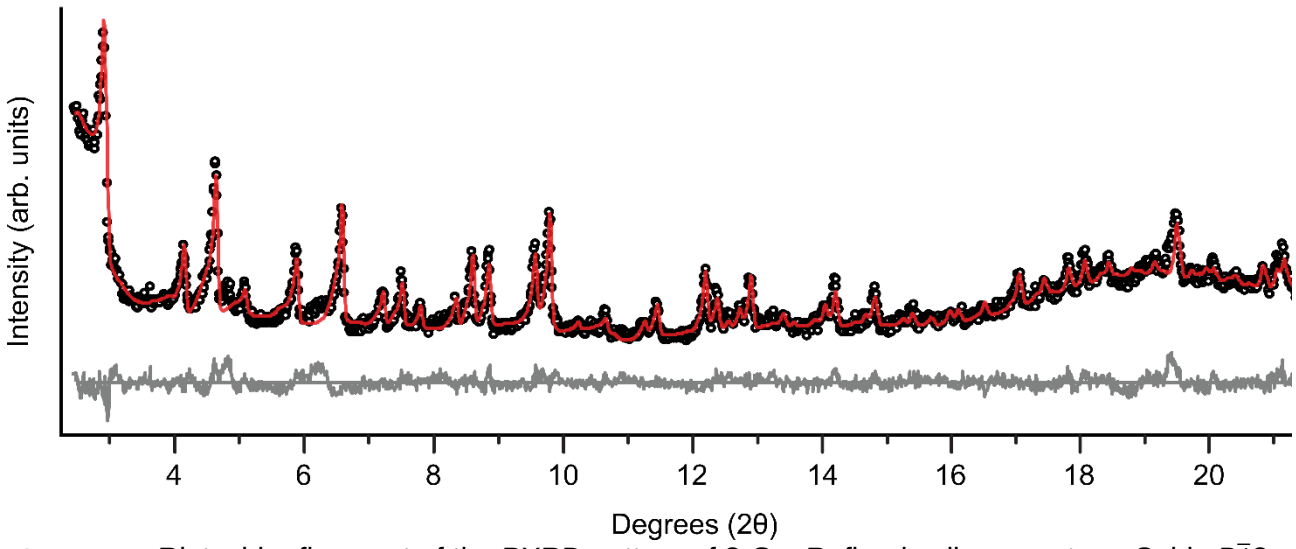

Figure S12. Rietveld refinement of the PXRD pattern of **3·Cu**. Refined cell parameters: Cubic $P\bar{4}3n$, a = 42.23 Å; α = 90°. For comparison, the cell parameters of the X-ray structure are: a = 41.18 Å; α = 90°.

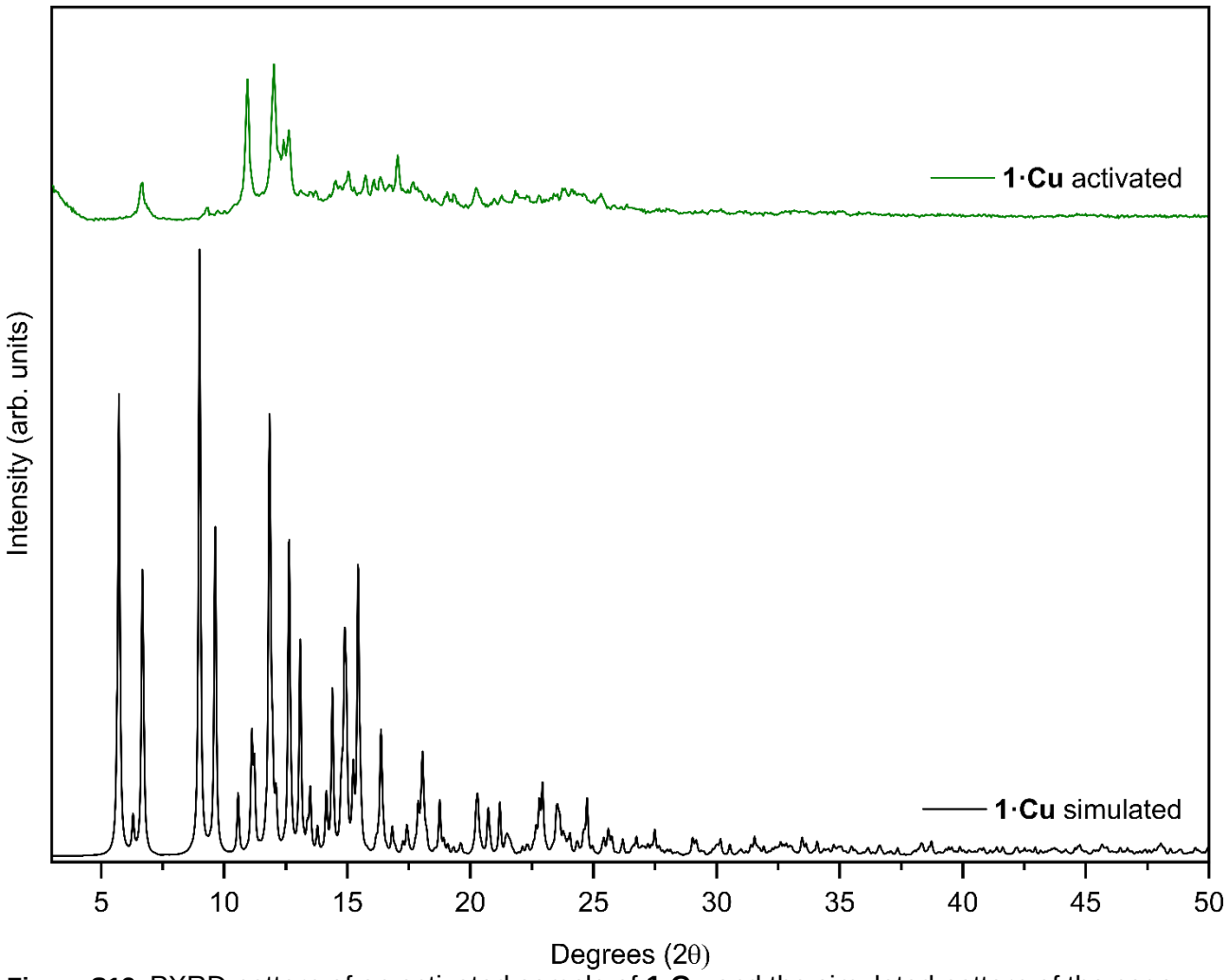

Figure S13. PXRD pattern of an activated sample of **1·Cu** and the simulated pattern of the cage.

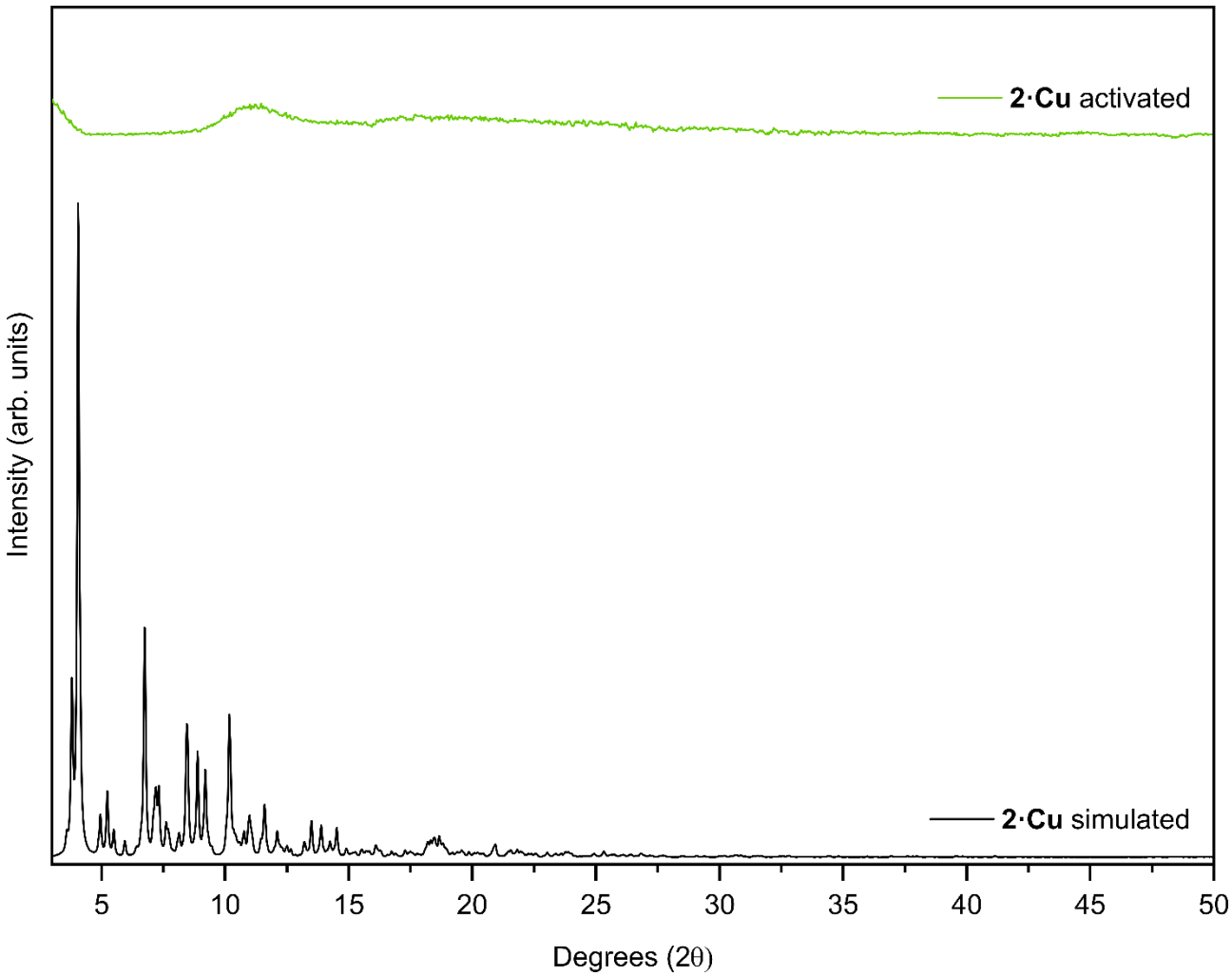

Figure S14. PXRD pattern of an activated sample of **2·Cu** and the simulated pattern of the cage.

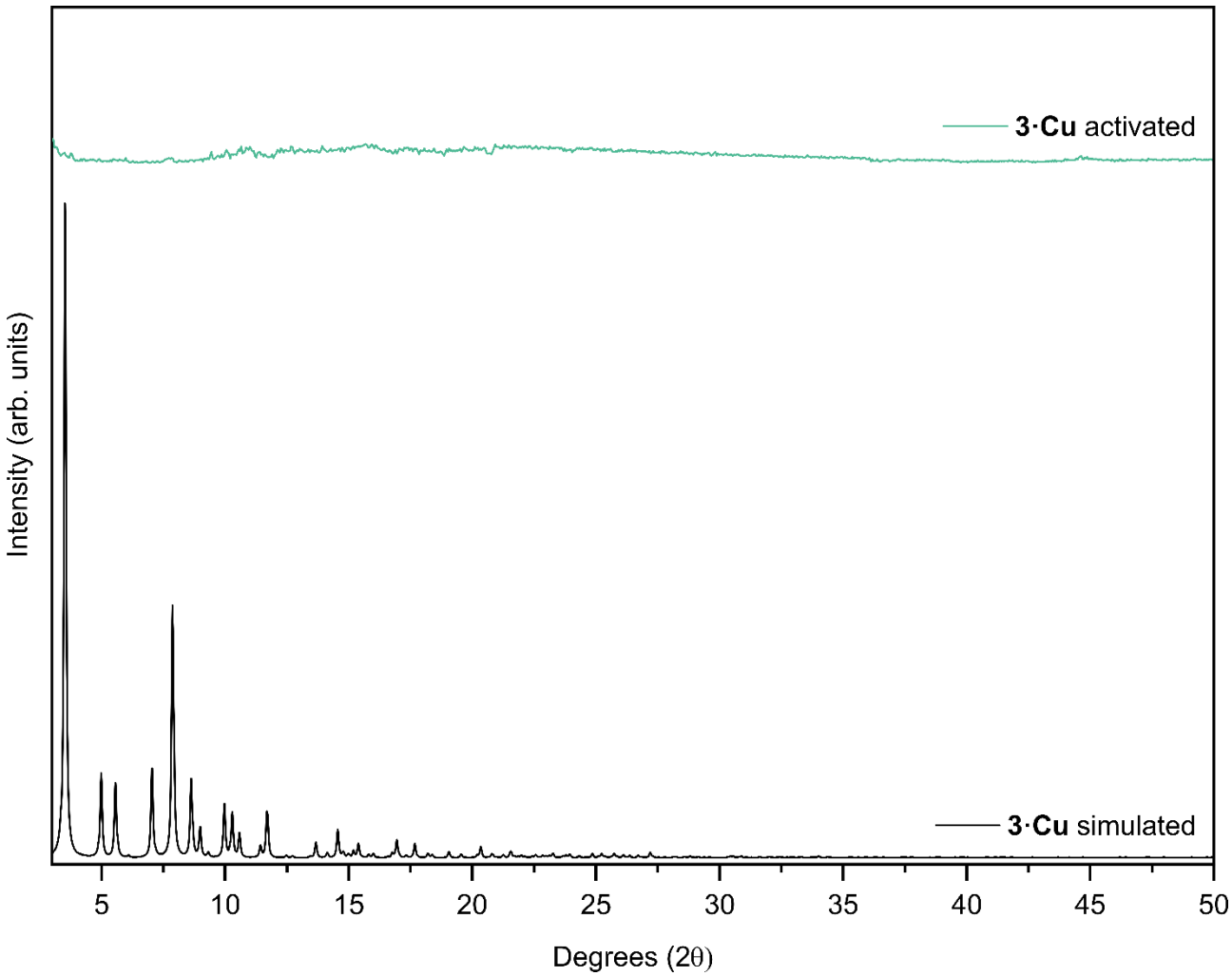

Figure S15. PXRD pattern of an activated sample of **3·Cu** and the simulated pattern of the cage.

3. Thermal gravimetric analysis

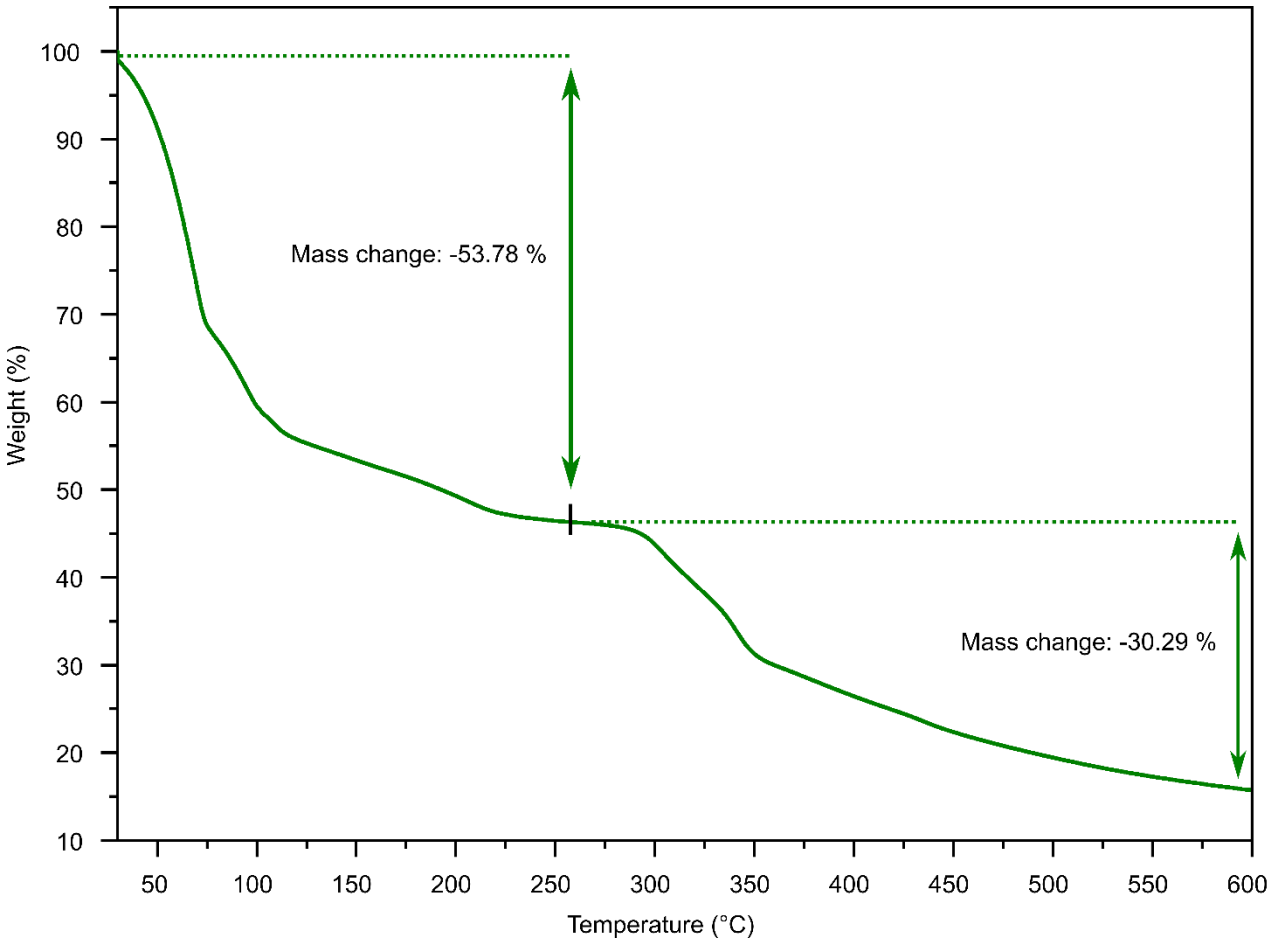

Figure S16. TGA trace of **1·Cu** (DMF solvated sample).

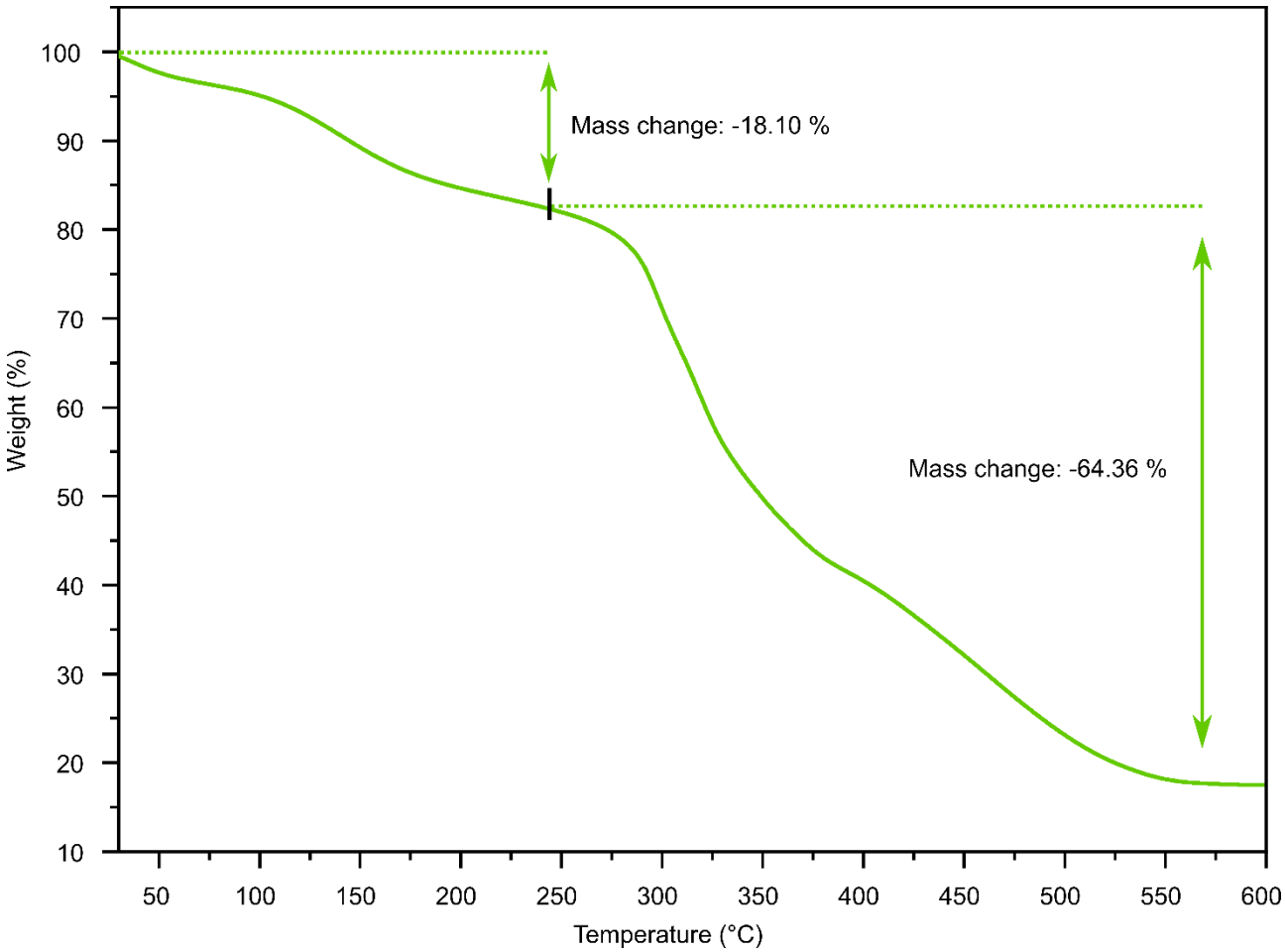

Figure S17. TGA trace of **2·Cu** (acetone solvated sample).

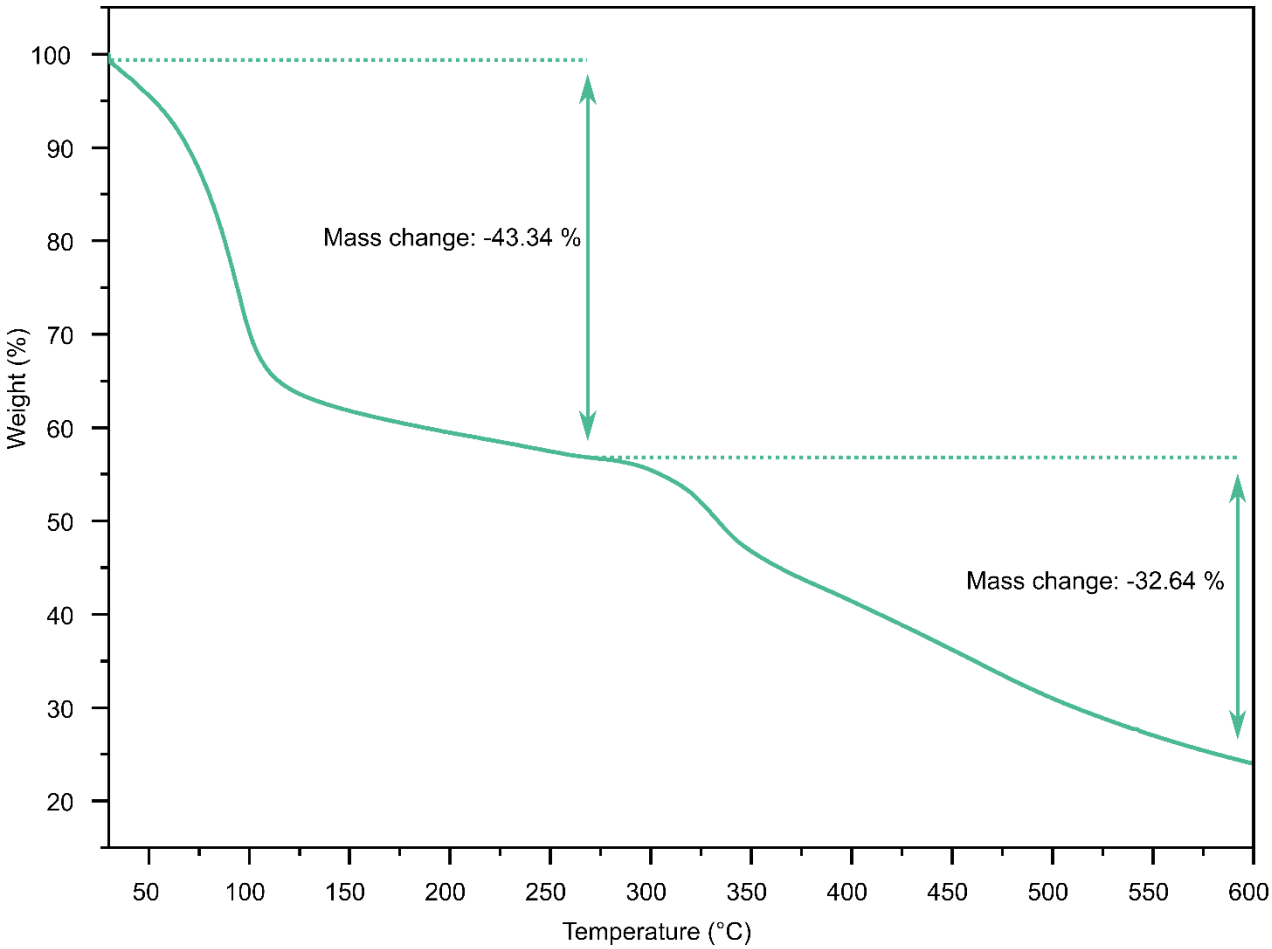

Figure S18. TGA trace of **3·Cu** (DMF solvated sample).

4. Gas adsorption

Prior to activation, samples were repeatedly soaked in acetone (x 5) over a period of 24 h. The samples were then activated directly in adsorption measurement tubes, where they were heated on an aluminum heat block at 120 °C under vacuum for 6 h prior to analysis.

Table S1. Surface areas (m^2/g) as calculated from the N_2 77 K and CO_2 195 K isotherms.

Samples	**N_2 77 K SA_{BET} (m^2/g)**	**CO_2 195 K SA_{BET} (m^2/g)**
1·Cu	101.4 ± 0.6	70.1 ± 1.3
2·Cu	19.5 ± 0.2	100.5 ± 0.6

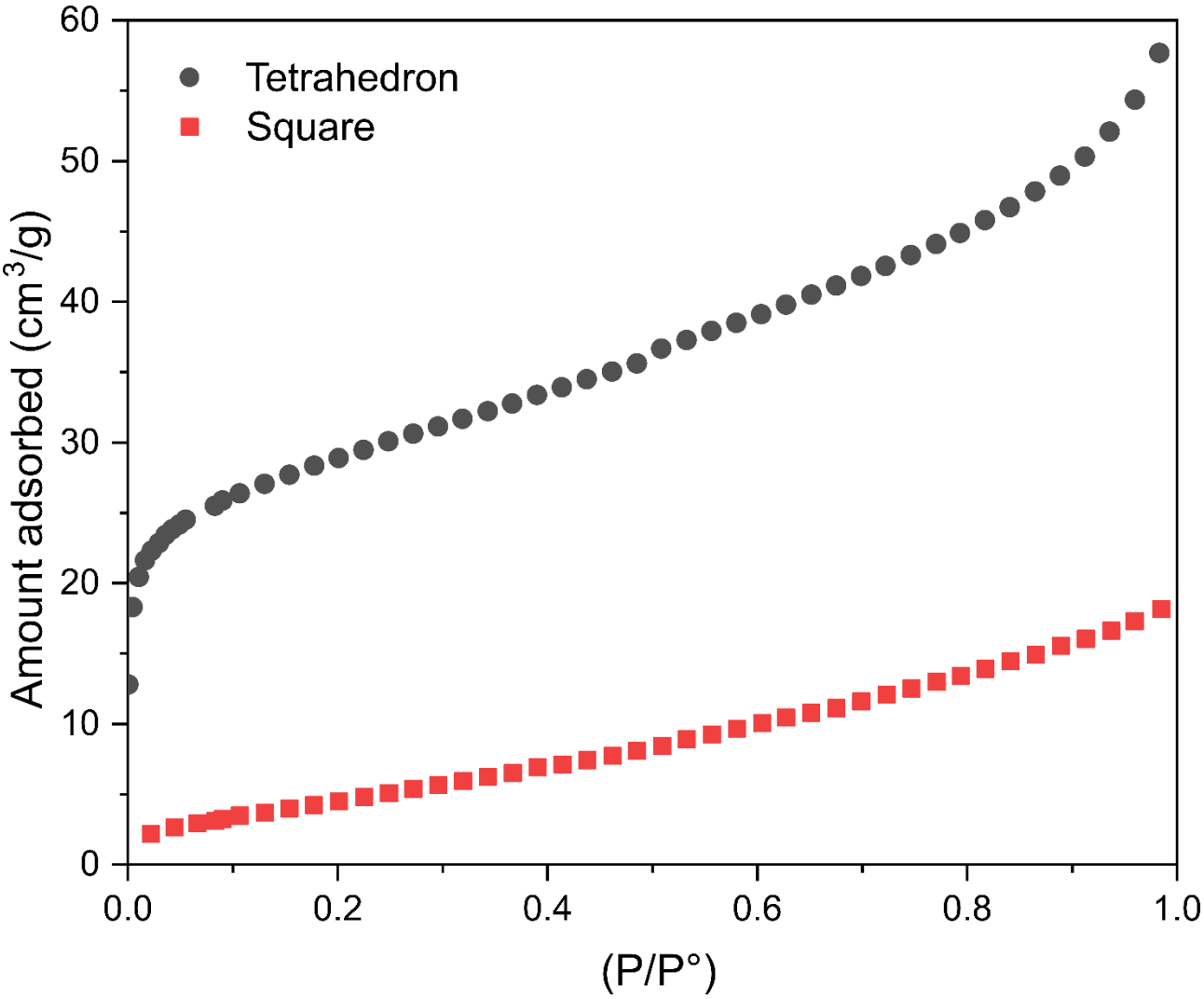

Figure S19. N_2 77 K isotherm of **1·Cu** and **2·Cu.**

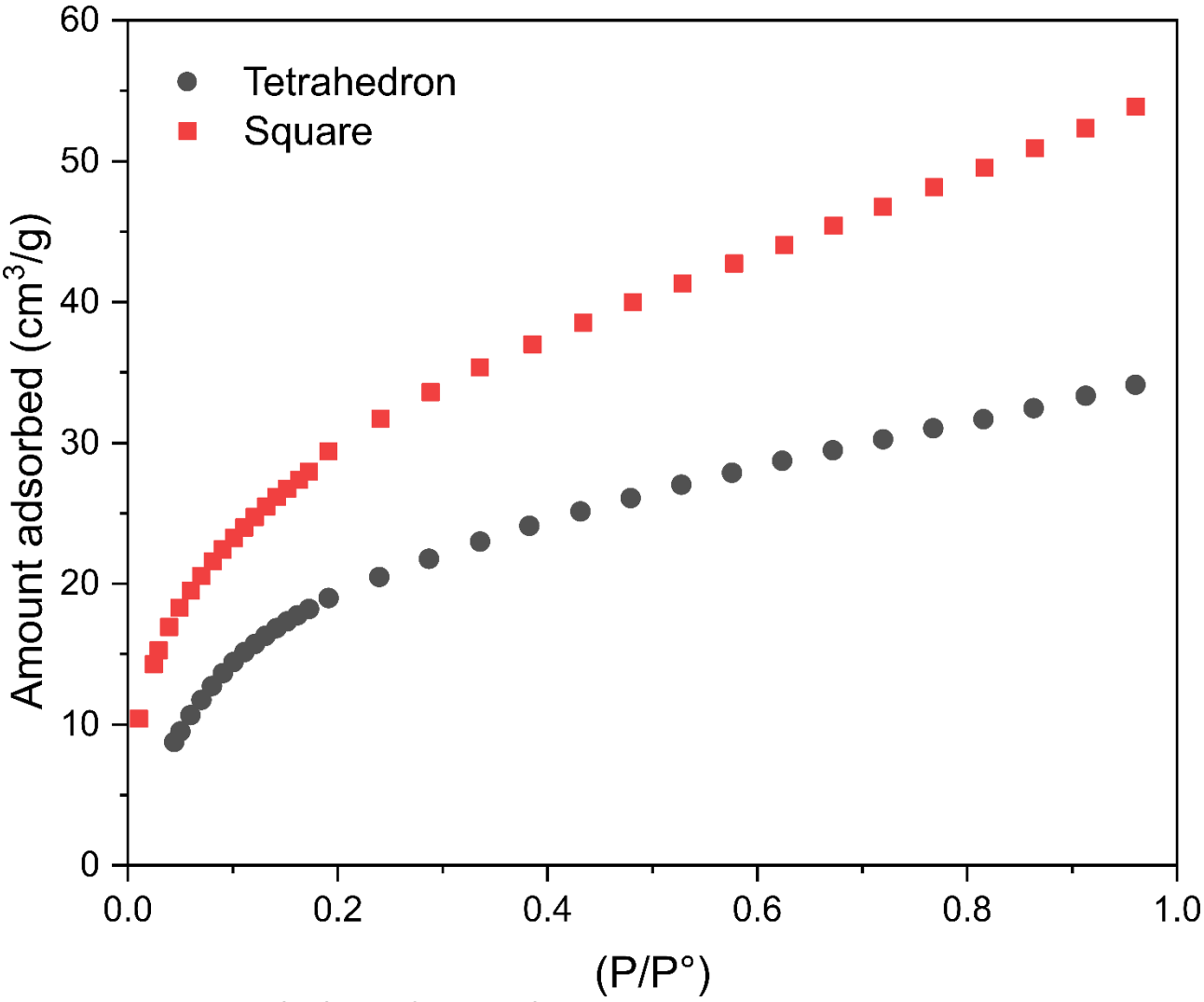

Figure S20. CO_2 195 K isotherm of **1·Cu** and **2·Cu**.

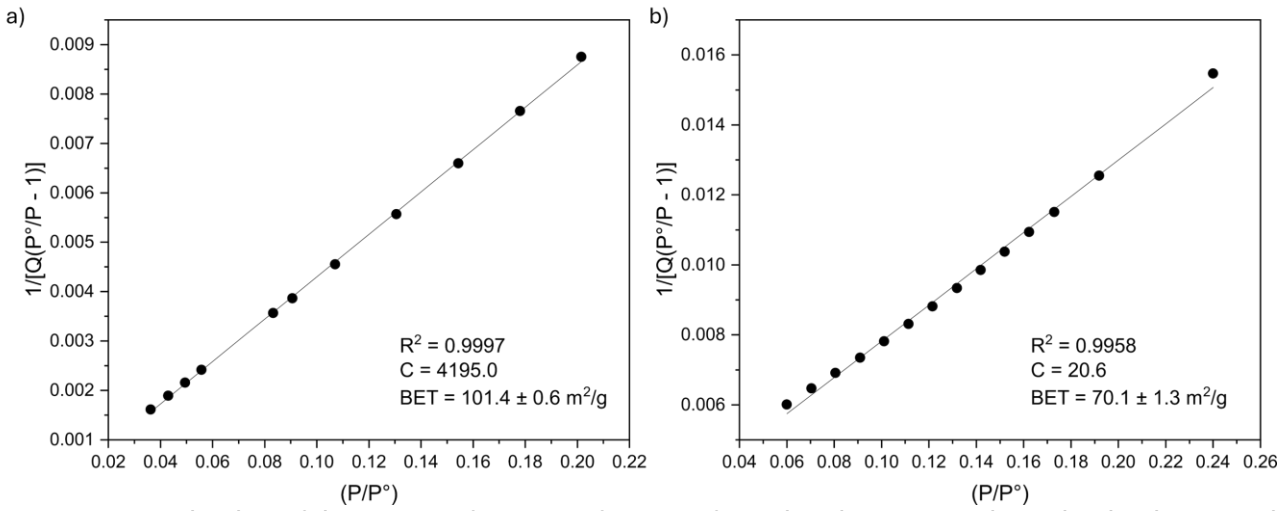

Figure S21. Derivation of the BET surface area for **1·Cu** from the a) 77 K N_2 adsorption isotherm and b) 195 K CO_2 adsorption isotherm.

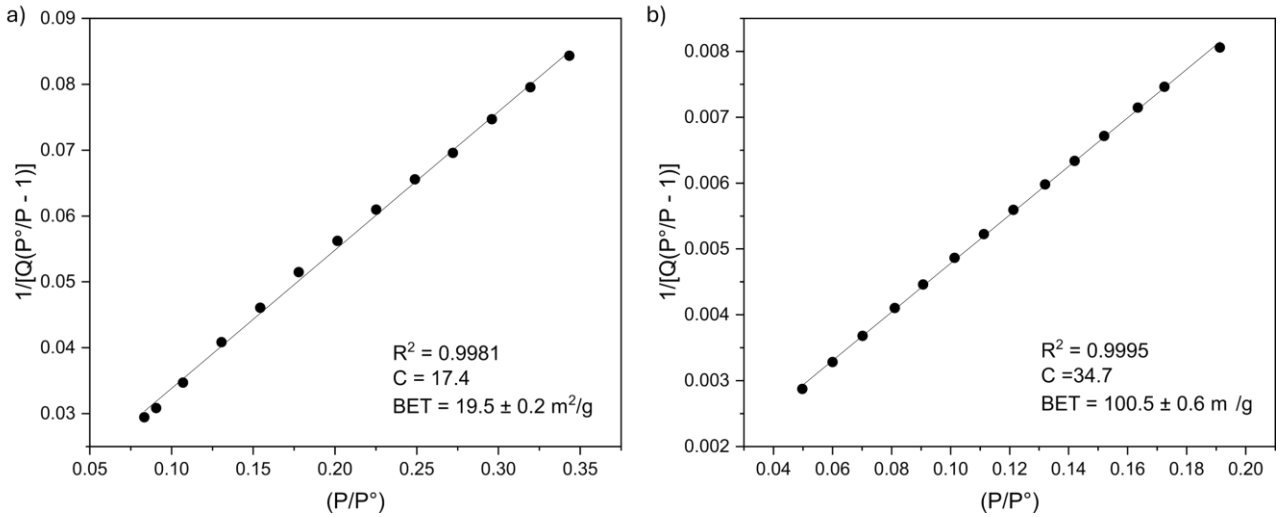

Figure S22. Derivation of the BET surface area for **2·Cu** from the a) 77 K N_2 adsorption isotherm and b) 195 K CO_2 adsorption isotherm.

5. X-ray crystallography

5.1. General methods

Single crystals were mounted in paratone-N oil on a plastic loop. X-ray diffraction data for **1·Cu**, **2·Cu**, **3·Cu**, **1·Rh**, and **2·Rh** were collected at 100(2) K on the MX-1 or MX-2 beamlines of the Australian Synchrotron.[5,6] Structures were solved by direct methods using SHELXT[7] and refined with SHELXL[8] and ShelXle[9] as a graphical user interface. All non-hydrogen atoms were refined anisotropically and hydrogen atoms were included as invariants at geometrically estimated positions. X-ray experimental data is given in Table S2.

*5.1.1. Specific refinement details for **1·Cu***

Stereochemical restraints DMF solvent molecules were generated by the GRADE program using the GRADE Web Server (http://grade.globalphasing.org) and applied in the refinement. A GRADE dictionary for SHELXL contains target values and standard deviations for 1,2-distances (DFIX) and 1,3-distances (DANG). This helped to produce a stable model of the DMF solvent. The refinement of ADP's for carbon, nitrogen and oxygen atoms was aided by similarity restraints (SIMU).[10] The contribution of the electron density from disordered, pore-bound solvent molecules, which could not be modelled with discrete atomic positions were handled using the SQUEEZE[11] routine in PLATON,[12] which strongly improved all figures of merit (FOM).

*5.1.2. Specific refinement details for **2·Cu***

Stereochemical restraints for L^2, and DEA solvent molecules were generated by the GRADE program using the GRADE Web Server (http://grade.globalphasing.org) and applied in the refinement. A GRADE dictionary for SHELXL contains target values and standard deviations for 1,2-distances (DFIX) and 1,3-distances (DANG), as well as restraints for planar groups (FLAT). This helped to produce a stable model of the DEA solvent and aided in developing a model for the ligand components with more precise C-C bonds. All displacements for non-hydrogen atoms were refined anisotropically. The refinement of ADP's for carbon, nitrogen and oxygen atoms was enabled by a combination of similarity restraints (SIMU).[10] The contribution of the electron density from disordered, pore-bound solvent molecules, which could not be modelled with discrete atomic positions were handled using the SQUEEZE[11] routine in PLATON,[12] which strongly improved all figures of merit (FOM).

*5.1.3. Specific refinement details for **3·Cu***

Stereochemical restraints for L^3 were generated by the GRADE program using the GRADE Web Server (http://grade.globalphasing.org) and applied in the refinement. A GRADE dictionary for SHELXL contains target values and standard deviations for 1,2-distances (DFIX) and 1,3-distances (DANG), as well as restraints for planar groups (FLAT). This aided in developing a model for the ligand components with more precise C-C bonds. All displacements for non-hydrogen atoms were refined anisotropically. The refinement of ADP's for carbon, nitrogen and oxygen atoms was enabled by a combination of similarity restraints (SIMU).[10] The contribution of the electron density from disordered, pore-bound solvent molecules, which could not be modelled with discrete atomic positions were handled using the SQUEEZE[11] routine in PLATON,[12] which strongly improved all figures of merit (FOM).

*5.1.4. Specific refinement details for **1·Rh***

Stereochemical restraints for L^1, and DMF solvent molecules were generated by the GRADE program using the GRADE Web Server (http://grade.globalphasing.org) and applied in the refinement. A GRADE dictionary for SHELXL contains target values and standard deviations for 1,2-distances (DFIX) and 1,3-distances (DANG), as well as restraints for planar groups (FLAT). This helped to produce a stable model of the DMF solvent and aided in developing a model for the ligand components with more precise C-C bonds. All displacements for non-hydrogen atoms were refined anisotropically. The refinement of ADP's for carbon, nitrogen and oxygen atoms was enabled by a combination of similarity restraints (SIMU).[10] The contribution of the electron density from disordered, pore-bound solvent molecules, which could not be modelled with discrete atomic positions were handled using the SQUEEZE[11] routine in PLATON,[12] which strongly improved all figures of merit (FOM).

*5.1.5. Specific refinement details for **2·Rh***

Stereochemical restraints for L^{p2}, and DMA solvent molecules were generated by the GRADE program using the GRADE Web Server (http://grade.globalphasing.org) and applied in the refinement. A GRADE dictionary for SHELXL contains target values and standard deviations for 1,2-distances (DFIX) and 1,3-distances (DANG), as well as restraints for planar groups (FLAT). This helped to produce a stable model of the DMA solvent and aided in developing a model for the ligand components with more precise C-C bonds. All displacements for non-hydrogen atoms were refined anisotropically. The refinement of ADP's for carbon, nitrogen and oxygen atoms was enabled by a combination of similarity restraints (SIMU).[10] The contribution of the electron density from disordered, pore-bound solvent molecules, which could not be modelled with discrete atomic positions were handled using the SQUEEZE[11] routine in PLATON,[12] which strongly improved all figures of merit (FOM).

Table S1. Disordered solvent removed from the formula unit by the SQUEEZE process.

Structure	**1·Cu**	**2·Cu**	**3·Cu**	**1·Rh**	**2·Rh**
Void count electrons in unit cell[a]	883	4382	11673	1204	7858
Z	2	4	8	2	4
Solvent content per formula unit[b]	10 × DMF 4 × H_2O	16.5 × DEA 4 × H_2O	35 × DMF 6 × H_2O	14 × DMF 4 × H_2O	40 × DMA 4.5 × H_2O

[a] _platon_squeeze_void_count_electrons

[b] solvent content based on reaction solvent

Table S2. X-ray experimental data for **1·Cu**, **2·Cu** and **3·Cu**.

Compound	**1·Cu**	**2·Cu**	**3·Cu**
CCDC number	2372768	2372767	2372771
Empirical formula	$C_{165}H_{145}Cu_8N_7O_{55}$	$C_{264}H_{212}Cu_8N_4O_{56}$	$C_{204}H_{120}Cu_6O_{42}$
Formula weight	3614.19	4844.68	3624.23
Crystal system	Monoclinic	Monoclinic	Cubic
Space group	$P2_1/m$	$P2_1/c$	P-43n
a (Å)	19.340(4)	28.7693(3)	41.178(5)
b (Å)	29.811(6)	53.8990(8)	41.178(5)
c (Å)	19.575(4)	31.4036(3)	41.178(5)
α (°)	90	90	90
β (°)	113.53(3)	97.1090(10)	90
γ (°)	90	90	90
Volume ($Å^3$)	10348(4)	48321.2(10)	69823(24)
Z	2	4	8
Density (calc.) (Mg/m^3)	1.418	0.937	1.197
Absorption coefficient (mm^{-1})	0.897	0.857	0.438
F(000)	4592	14400	26512
Crystal size (mm^3)	0.18 x 0.14 x 0.04	0.18 x 0.17 x 0.04	0.24 x 0.23 x 0.21
θ range for data collection (°)	1.135 to 27.129	2.764 to 56.893	0.699 to 19.802
Reflections collected	174128	257707	393023
Observed reflections [R(int)]	23197 [0.0566]	63356 [0.0695]	10584 [0.1544]
Goodness-of-fit on F^2	1.088	1.236	1.039
R_1 [$I>2\sigma(I)$]	0.0871	0.1050	0.0537
wR_2 (all data)	0.2854	0.3703	0.1674
Largest diff. peak and hole ($e.Å^{-3}$)	1.495 and -1.141	0.861 and -0.376	0.275 and -0.175
Data / restraints / parameters	23197 / 1045 / 1239	63356 / 3560 / 3030	10584 / 827 / 758

Table S3. X-ray experimental data for **1·Rh** and **2·Rh**

Compound	**1·Rh**	**2·Rh**
CCDC number	2372769	2372770
Empirical formula	$C_{153}H_{117}N_3O_{56}Rh_8$	$C_{296}H_{276}N_6O_{56}Rh_8$
Formula weight	3716.77	5636.49
Crystal system	Monoclinic	Monoclinic
Space group	$P2_1/m$	C2/c
a (Å)	19.541(4)	59.811(12)
b (Å)	30.103(6)	20.955(4)
c (Å)	19.898(4)	50.565(10)
α (°)	90	90
β (°)	114.14(3)	121.04(3)
γ (°)	90	90
Volume (Å^3)	10681(4)	54300(24)
Z	2	4
Density (calc.) (Mg/m^3)	1.496	1.126
Absorption coefficient (mm^{-1})	0.694	0.307
F(000)	4928	19468
Crystal size (mm^3)	0.18 x 0.14 x 0.12	0.17 x 0.16 x 0.04
θ range for data collection (°)	1.121 to 23.357	0.863 to 23.350
Reflections collected	78784	258776
Observed reflections [R(int)]	13321 [0.0956]	38575 [0.1021]
Goodness-of-fit on F^2	1.071	1.069
R_1 [$I>2\sigma(I)$]	0.0829	0.0680
wR_2 (all data)	0.2988	0.2385
Largest diff. peak and hole (e.Å^{-3})	0.853 and -0.670	0.850 and -0.549
Data / restraints / parameters	13321 / 2010 / 983	38575 / 1855 / 1708

5.1. X-ray structures

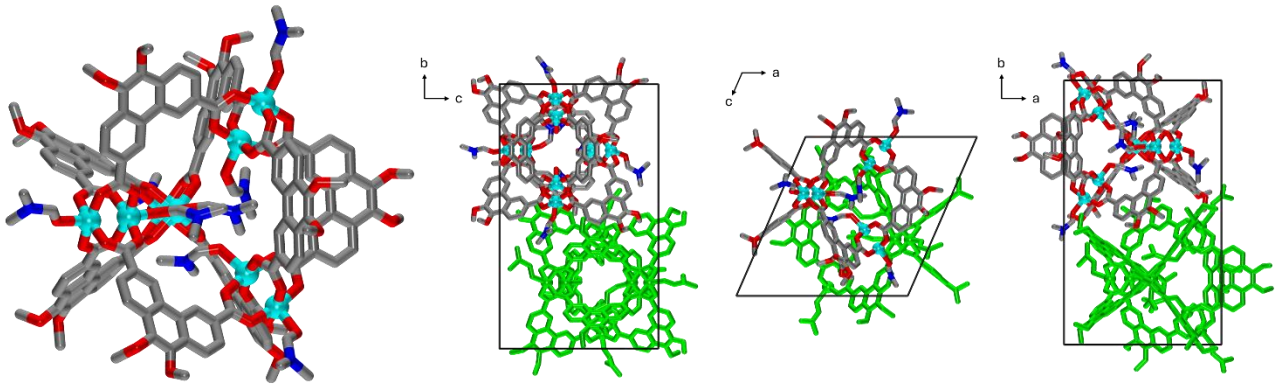

Figure S23. X-ray structure of **1·Cu** with hydrogen atoms removed for clarity, as well as the unit cell viewed along the a, b and c-axes (C, grey; N, dark blue; O, red; Cu, cyan).

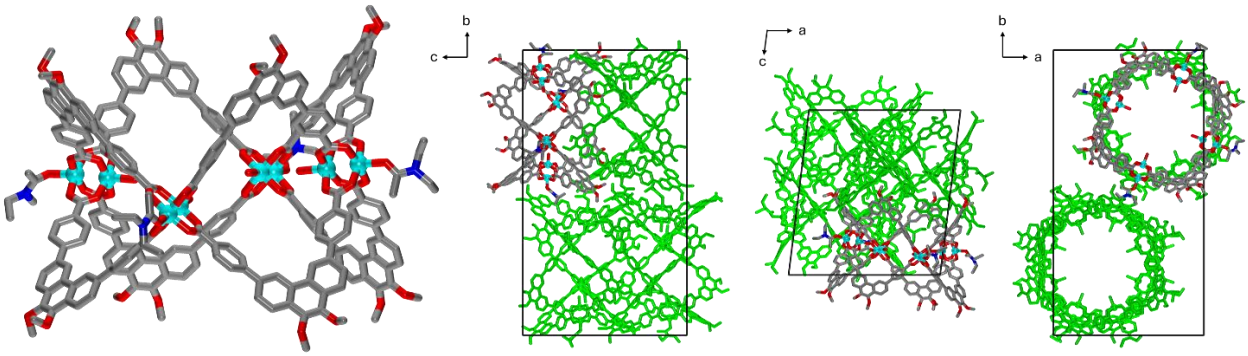

Figure S24. X-ray structure of **2·Cu** with hydrogen atoms removed for clarity, as well as the unit cell viewed along the a, b and c-axes (C, grey; N, dark blue; O, red; Cu, cyan).

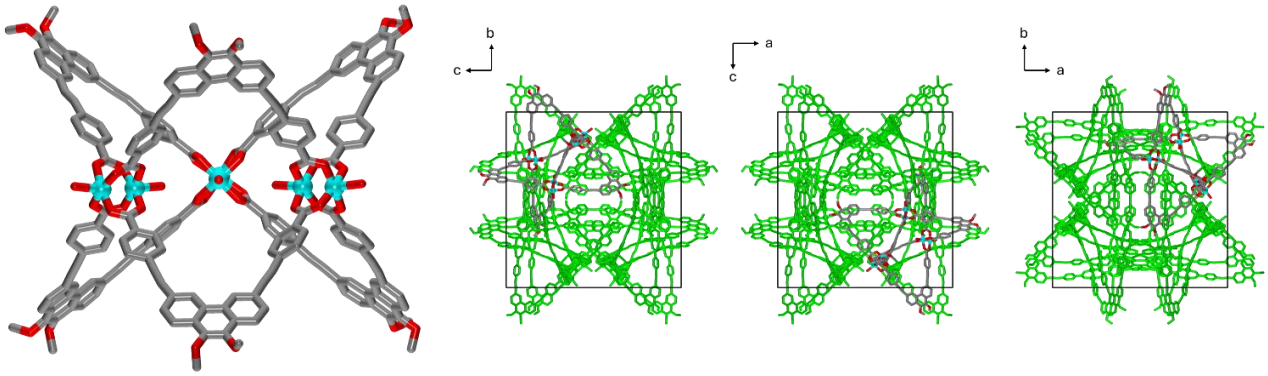

Figure S25. X-ray structure of **3·Cu** with hydrogen atoms removed for clarity, as well as the unit cell viewed along the a, b and c-axes (C, grey; O, red; Cu, cyan).

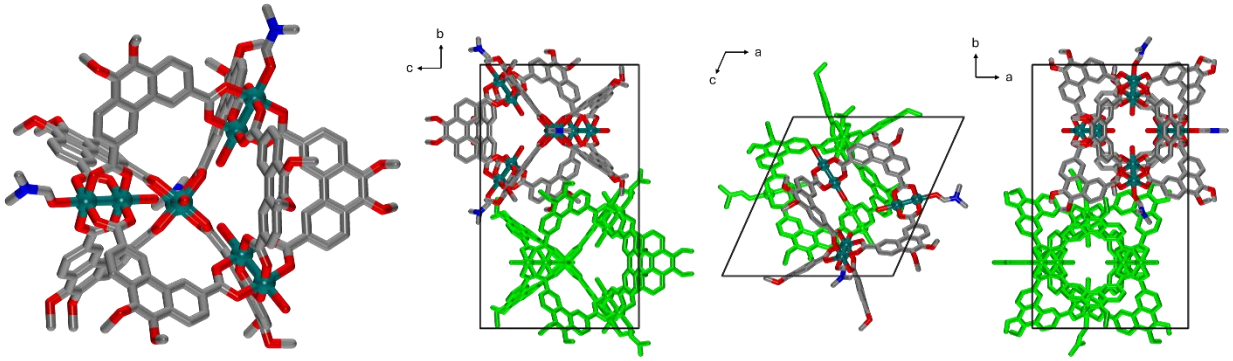

Figure S26. X-ray structure of **1·Rh** with hydrogen atoms removed for clarity, as well as the unit cell viewed along the a, b and c-axes (C, grey; N, dark blue; O, red; Rh, teal).

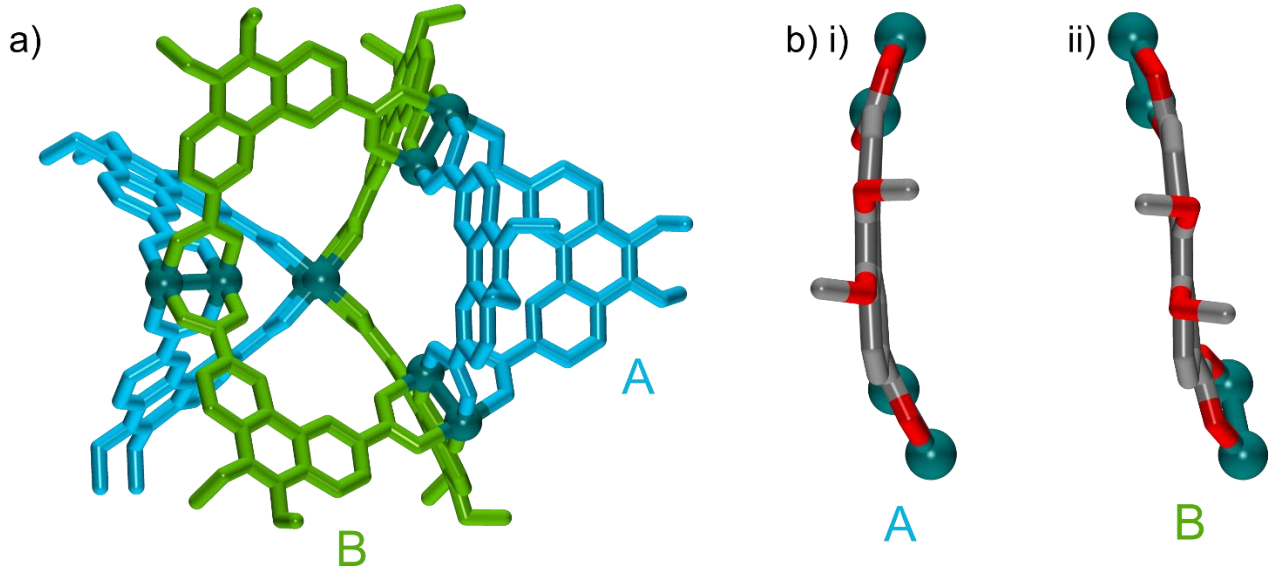

Figure S27. X-ray structure of (a) **1·Rh** with hydrogen atoms removed for clarity which distinguishes the two environments of L^1; blue (A): two ligands originating from one Rh-paddlewheel cluster and ending at the same cluster; and green (B): two ligands originating from one Rh-paddlewheel cluster and ending at different clusters; and (b) the two types of geometries L^1 adopts, (i) and (ii) (C, grey; N, dark blue; O, red; Rh, teal).

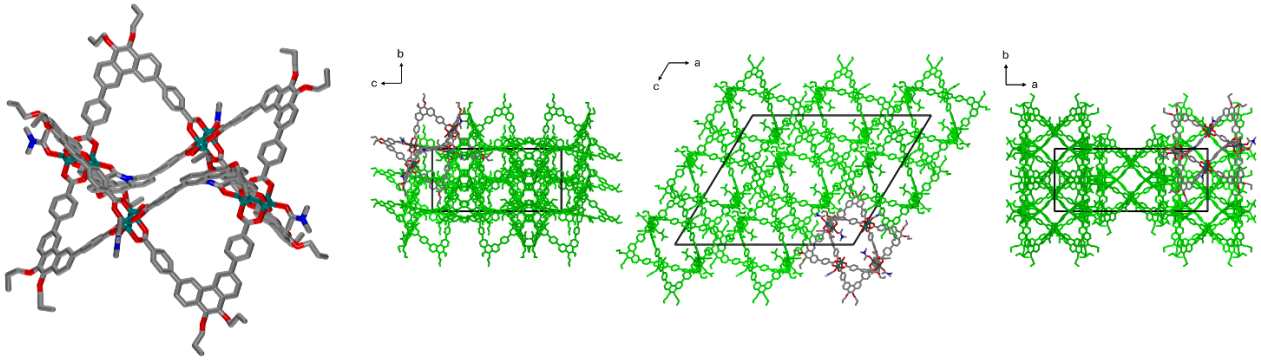

Figure S28. X-ray structure of **2·Rh** with hydrogen atoms removed for clarity, as well as the unit cell viewed along the a, b and c-axes (C, grey; N, dark blue; O, red; Rh, teal).

5.2. Thermal ellipsoid plots

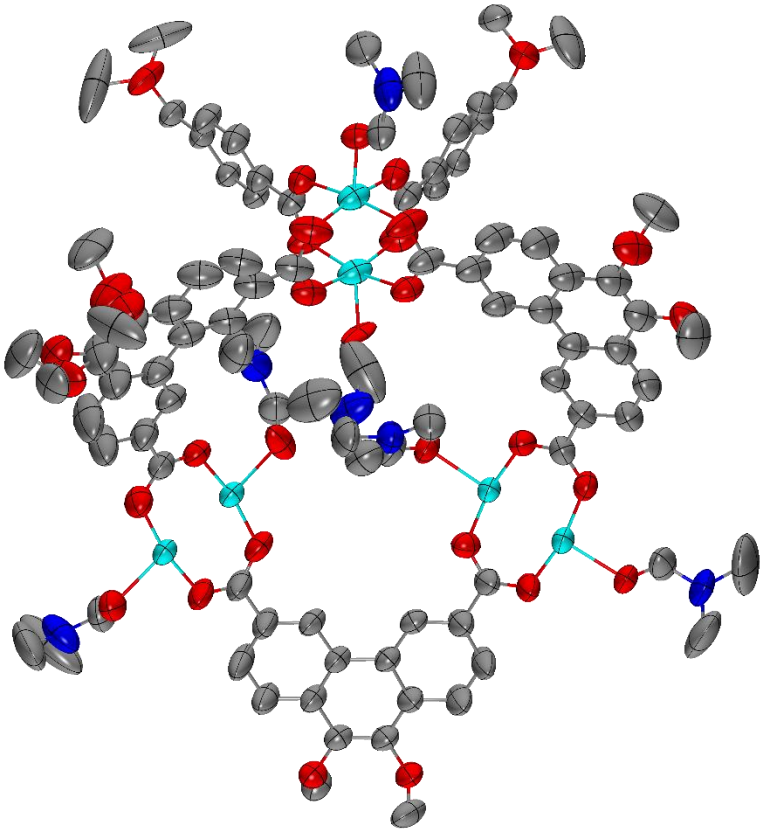

Figure S29. The asymmetric unit of the X-ray structures of **1·Cu** with all non-hydrogen atoms shown as ellipsoids at the 50% probability level (C, grey; N, dark blue; O, red; Cu, cyan).

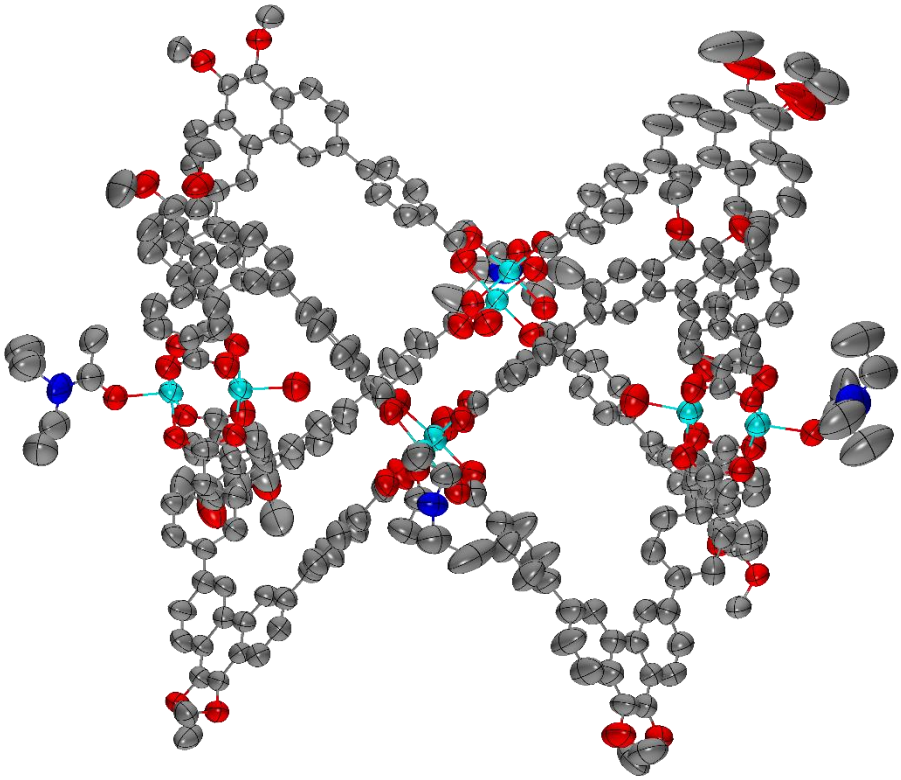

Figure S30. The asymmetric unit of the X-ray structures of **2·Cu** with all non-hydrogen atoms shown as ellipsoids at the 50% probability level (C, grey; N, dark blue; O, red; Cu, cyan).

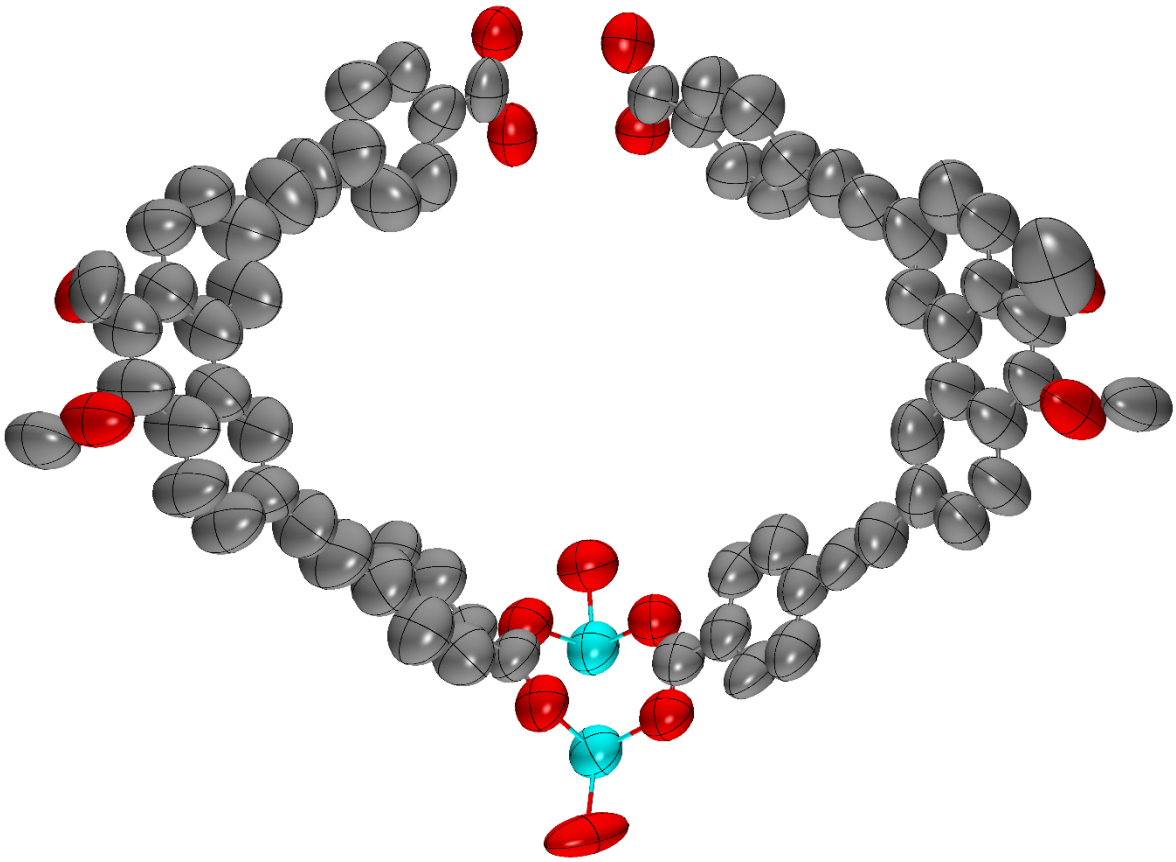

Figure S31. The asymmetric unit of the X-ray structure of **3·Cu** with all non-hydrogen atoms shown as ellipsoids at the 50% probability level (C, grey; O, red; Cu, cyan).

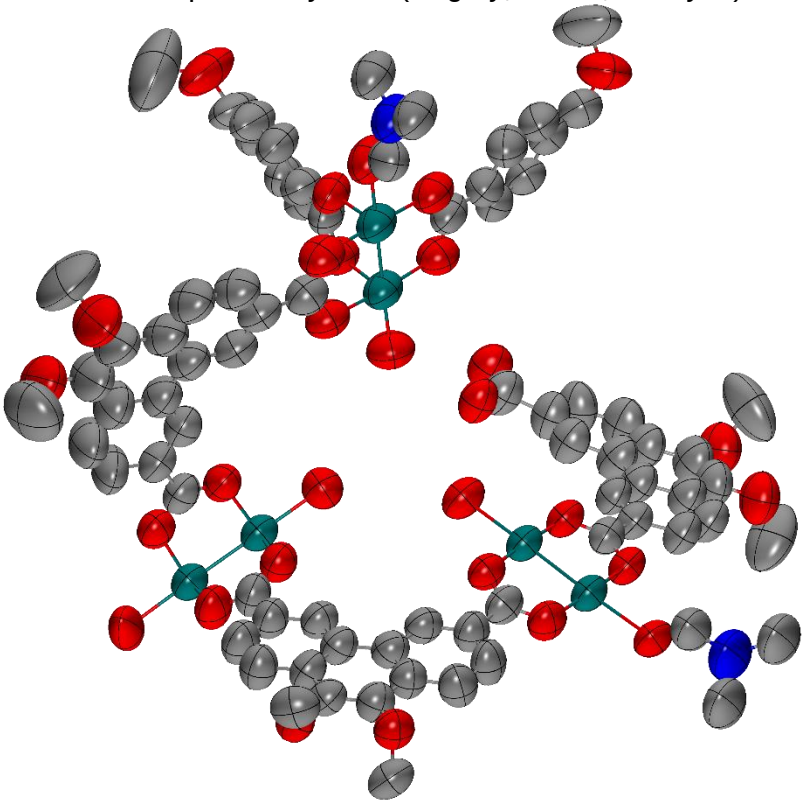

Figure S32. The asymmetric unit of the X-ray structure of **1·Rh** with all non-hydrogen atoms shown as ellipsoids at the 50% probability level (C, grey; N, dark blue; O, red; Rh, teal).

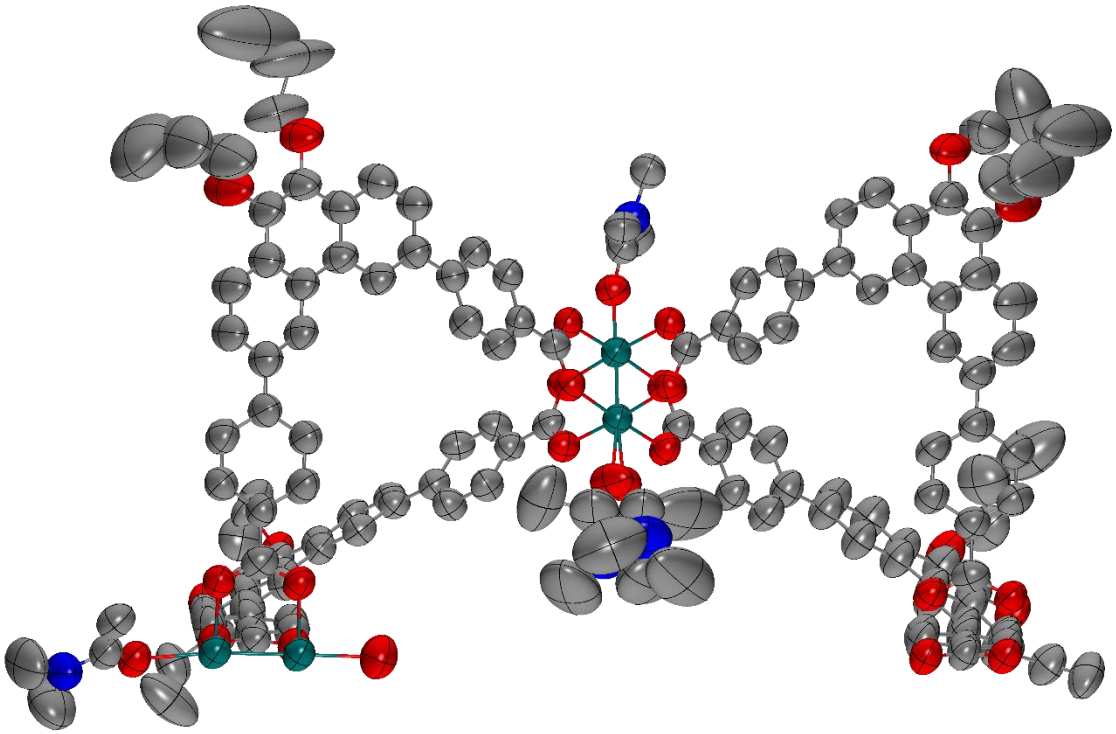

Figure S33. The asymmetric unit of the X-ray structure of **2·Rh** with all non-hydrogen atoms shown as ellipsoids at the 50% probability level (C, grey; N, dark blue; O, red; Rh, teal).

6. DFT calculations

Density Functional Theory (DFT) calculations have been carried out for Cu-paddlewheel cluster MOCs, Vienna ab−initio Simulation Package (VASP).[13] A generalized gradient approximation Perdew-Burke-Ernzerhof (PBE) functional has been used to describe all ionic-electronic interactions between the atoms and ions.[14] All the atoms in the Cu-paddlewheel MOCs are allowed to relax with γ-point sampling. The individual units comprising the MOCs (table S5) as well as the three potential MOCs themselves (table S6) are depicted below. A plane-wave energy cutoff of 400 eV with DFT-D3 dispersion approach for including the long-range forces has been considered to relax all systems until the energies and atomic forces converge to 10^{-3} eV/atom and 0.05 eV/Å, respectively.[15]

To calculate the feasibility of formation of each Cu-cluster MOC with the 3 ligands, their formation energy w.r.t. per $Cu_2(OAc)_4$ cluster has been calculated as:

$$E_{form/cluster} = \frac{E_{complex} - n * E_{Cu-cluster} - 2n * E_{ligand} + 4n * E_{H_2}}{n}$$

where, n is the number of $Cu_2(OAc)_4$ clusters in the complex (e.g. n=3 for triangular complex). The $E_{form/cluster}$ (in eV) for each ligand when coordinated in different geometries are tabulated in table S4.

Table S4. Formation energies of the tetrahedral, double-walled square and double-walled triangle MOC topologies for L^1, L^2 and L^3.

$E_{form/cluster}$ (eV)	Tetrahedron (M_8L_8)	Square (M_8L_8)	Triangle (M_6L_6)
L^1	-1.27	-2.10	-1.80
L^2	-1.22	-1.49	-1.39
L^3	-0.71	-0.83	-1.11

Table S5. Individual units used to build the different potential Cu-cluster MOC topologies.

$Cu_2(OAc)_4$	L^1	L^2	L^3
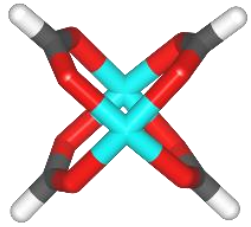	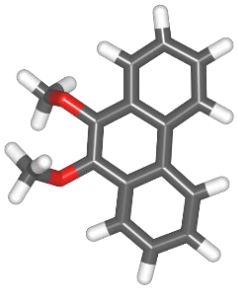	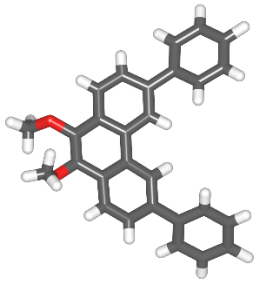	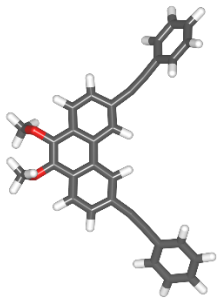

Table S6. Generated structures of each potential Cu-cluster MOC topology for L^1, L^2 and L^3.

Cage/Ligand	Tetrahedron (M_8L_8)	Square (M_8L_8)	Triangle (M_6L_6)
L^1	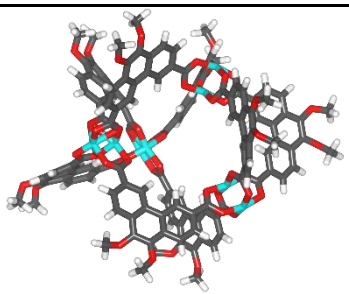	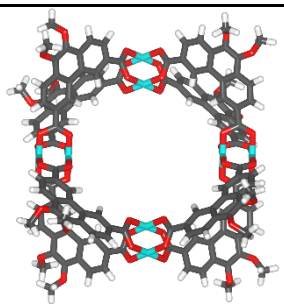	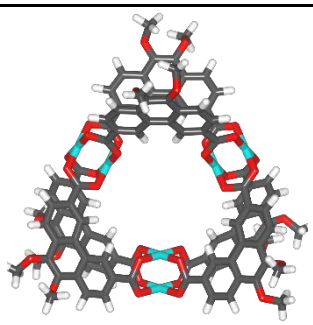
L^2	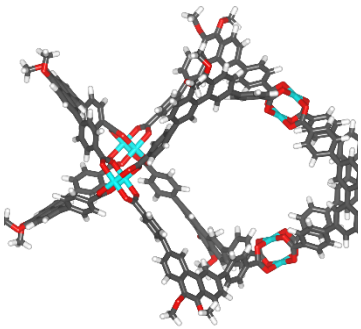	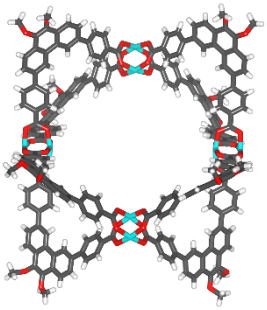	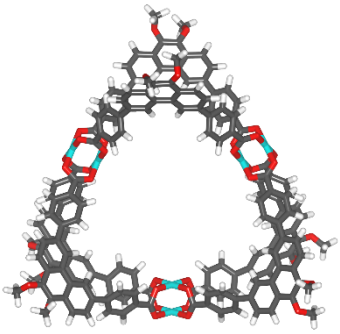
L^3	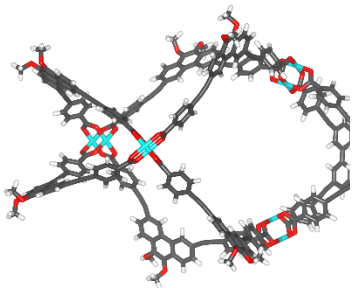	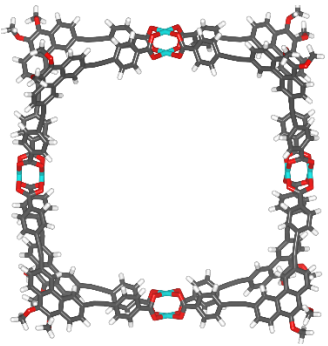	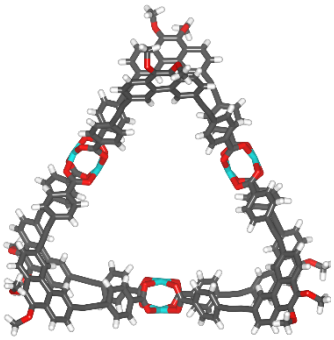

7. References

(1) Paruch, K.; Vyklicky, L.; Katz, T. J. PREPARATION OF 9,10-DIMETHOXYPHENANTHRENE AND 3,6- DIACETYL-9,10-DIMETHOXYPHENANTHRENE. *Organic Syntheses* **2003**, *80*, 227–232.

(2) Phulwale, B. V.; Mishra, S. K.; Nečas, M.; Mazal, C. Phenanthrylene-Butadiynylene and Phenanthrylene-Thienylene Macrocycles: Synthesis, Structure, and Properties. *J Org Chem* **2016**, *81* (15), 6244–6252. https://doi.org/10.1021/acs.joc.6b00814.

(3) Bloch, W. M.; Holstein, J. J.; Dittrich, B.; Hiller, W.; Clever, G. H. Hierarchical Assembly of an Interlocked M8L16 Container. *Angewandte Chemie International Edition* **2018**, *57* (19), 5534–5538. https://doi.org/https://doi.org/10.1002/anie.201800490.

(4) Sumii, Y.; Kotoku, N.; Fukuda, A.; Kawachi, T.; Sumii, Y.; Arai, M.; Kobayashi, M. Enantioselective Synthesis of Dictyoceratin-A (Smenospondiol) and -C, Hypoxia-Selective Growth Inhibitors from Marine Sponge. *Bioorg Med Chem* **2015**, *23* (5), 966–975. https://doi.org/https://doi.org/10.1016/j.bmc.2015.01.021.

(5) Cowieson, N. P.; Aragao, D.; Clift, M.; Ericsson, D. J.; Gee, C.; Harrop, S. J.; Mudie, N.; Panjikar, S.; Price, J. R.; Riboldi-Tunnicliffe, A.; Williamson, R.; Caradoc-Davies, T. MX1: A Bending-Magnet Crystallography Beamline Serving Both Chemical and Macromolecular Crystallography Communities at the Australian Synchrotron. *J Synchrotron Radiat* **2015**, *22* (1), 187–190.

(6) Aragao, D.; Aishima, J.; Cherukuvada, H.; Clarken, R.; Clift, M.; Cowieson, N. P.; Ericsson, D. J.; Gee, C. L.; Macedo, S.; Mudie, N.; Panjikar, S.; Price, J. R.; Riboldi-Tunnicliffe, A.; Rostan, R.; Williamson, R.; Caradoc-Davies, T. T. MX2: A High-Flux Undulator Microfocus Beamline Serving Both the Chemical and Macromolecular Crystallography Communities at the Australian Synchrotron. *J Synchrotron Radiat* **2018**, *25* (3), 885–891.

(7) Sheldrick, G. M. No Title. *Acta Crystallogr. Sect. A* **2015**, *71*, 3–8.

(8) Sheldrick, G. M. No Title. *Acta Crystallogr. Sect. C* **2015**, *71*, 3–8.

(9) Hubschle, C. B.; Sheldrick, G. M.; Dittrich, B. ShelXle: A Qt Graphical User Interface for SHELXL. *J Appl Crystallogr* **2011**, *44* (6), 1281–1284. https://doi.org/doi:10.1107/S0021889811043202.

(10) Thorn, A.; Dittrich, B.; Sheldrick, G. M. Enhanced Rigid-Bond Restraints. *Acta Crystallographica Section A* **2012**, *68* (4), 448–451. https://doi.org/doi:10.1107/S0108767312014535.

(11) Spek, A. PLATON SQUEEZE: A Tool for the Calculation of the Disordered Solvent Contribution to the Calculated Structure Factors. *Acta Crystallogr. Sect. C* **2015**, *71* (1), 9–18. https://doi.org/doi:10.1107/S2053229614024929.

(12) Spek, A. Structure Validation in Chemical Crystallography. *Acta Crystallographica Section D* **2009**, *65* (2), 148–155. https://doi.org/doi:10.1107/S090744490804362X.

(13) Kresse, G.; Furthmüller, J. Efficiency of Ab-Initio Total Energy Calculations for Metals and Semiconductors Using a Plane-Wave Basis Set. *Comput Mater Sci* **1996**, *6* (1), 15–50. https://doi.org/https://doi.org/10.1016/0927-0256(96)00008-0.

(14) Perdew, J. P.; Burke, K.; Ernzerhof, M. Generalized Gradient Approximation Made Simple. *Phys Rev Lett* **1996**, *77* (18), 3865–3868. https://doi.org/10.1103/PhysRevLett.77.3865.

(15) Grimme, S.; Antony, J.; Ehrlich, S.; Krieg, H. A Consistent and Accurate Ab Initio Parametrization of Density Functional Dispersion Correction (DFT-D) for the 94 Elements H-Pu. *J Chem Phys* **2010**, *132* (15), 154104. https://doi.org/10.1063/1.3382344.